Forensic Science International 365 (2024) 112282

Contents lists available at ScienceDirect

Forensic Science International

journal homepage: www.elsevier.com/locate/forsciint

Analyzing 3D facial morphology: Insights from a comparative European and South African study on population affinity, sex, age, and allometry

Thandolwethu Mbali Mbonani *, Ericka Noelle L'Abbé, Alison Fany Ridel

University of Pretoria, Department of Anatomy, Faculty of Health Sciences, Tswelopele Building, Private Bag X323, Prinshof 349-Jr, Pretoria 0084, South Africa

ARTICLE INFO

Keywords:
Craniofacial variation
Geometric morphometric methods
Cone-beam computed tomography
3D reconstructions
Facial morphology matrices
Craniofacial reconstruction

ABSTRACT

Variable growth patterns and multifactorial mechanisms cause variation in facial shape. These differences in facial morphology pose challenges for craniofacial reconstruction. Three-dimensional (3D) imaging modalities are a valuable resource for examining these variations. In this study, we used geometric morphometric methods to evaluate the effects of population affinity, sex, age, and allometry on the variation and covariation of hard and soft tissue facial morphology matrices in a sample of French and white South African individuals. Seventy-six and 108 cone-beam computed tomography scans of white South African and French nationals, respectively, were retrospectively acquired. Three-dimensional anatomical structures (hard and soft tissue matrices) were extracted using MeVisLab© v. 2.7.1 software for dense landmarking of 43 craniometric, 50 capulometric, and 559 sliding landmarks. Geometric morphometric analyses were used to quantify shape differences attributed to population affinity, sex, age, and allometry and assess the covariation between hard tissue structures and soft facial tissues. Hard and soft tissue facial matrices were influenced by population differences, sexual dimorphism, and aging. Compared to sex and age, population affinity had the strongest influence on variation. In French individuals, all hard and soft tissue matrices were sexually dimorphic, except for the eyes and left external auditory meatus (EAM). In white South Africans, sexual dimorphism was observed for the mouth, midface, and left EAM. Significant shape differences were also observed for specific age groups. The underlying skull and overlying soft tissues were strongly associated with the nose and anterior nasal aperture (correlation, r^2-PLS = 0.976), followed by the right ear and right EAM (r^2-PLS = 0.875) and the left ear and left EAM (r^2-PLS = 0.871) in white South Africans. For French individuals, relatively weak to moderate correlations were observed, and the covariation between matrices was nonsignificant, except for the association between the right ear and right EAM (r^2-PLS = 0.499). The smallest covariation was observed between the mouth and midfacial matrix in both populations (South African: r^2-PLS = 0.464; French: r^2-PLS = 0.367), which was also nonsignificant. This study revealed that 3D imaging technology and geometric morphometric methods can accurately quantify and visualize facial morphology differences. These methods can also evaluate the association between skull structure and soft facial features.

1. Introduction

Every year, a substantial number, ranging between 7000 and 10,000 of unidentified bodies remain in South Africa's medico-legal laboratories, awaiting the meticulous process of identification [1]. This process hinges upon forensic methodologies, which compare antemortem and postmortem data, encompassing a spectrum from X-rays, DNA, to fingerprints, among other modalities [2]. However, the effectiveness of such methods encounters significant obstacles, particularly when faced with the scarcity of comparative records, complicating the identification process, notably in cases where the remains are unrecognizable due to decomposition, thermal destruction, or mutilation.

Craniofacial reconstruction (CFR) emerges as a viable alternative, influencing the anatomical foundation of the skull to reconstruct the facial appearance of a deceased individual [3,4]. The indispensability of the skull in CFR originates from its morphological distinctiveness, serving as a pivotal substrate for the recreation of facial features [5]. Nonetheless, the current state of CFR techniques often falters in accurately approximating facial appearance [6,7], a shortfall underscored by critics citing issues such as the references employed, lack of

* Corresponding author.
E-mail addresses: thandombonani83@gmail.com (T.M. Mbonani), ericka.labbe@up.ac.za (E.N. L'Abbé), alison.ridel@up.ac.za (A.F. Ridel).

https://doi.org/10.1016/j.forsciint.2024.112282
Received 28 November 2023; Received in revised form 25 March 2024; Accepted 28 October 2024
Available online 30 October 2024

standardization and the failure to account for population differences [7–10]. Traditionally established as a manual and time-consuming method [11–13], CFR has undergone a transformative evolution with the advent of 3D technologies, indicating improved precision and efficiency [2,9,13–19]. Technological strides, exemplified by cone-beam computed tomography (CBCT), afford unparalleled insights into craniofacial morphology, facilitating refined reconstructions and geometric morphometric (GMM) analyses. The utilization of GMM analyses holds promise in discovering subtle differentiations across diverse population groups, thereby accentuating the necessity for population-specific datasets to delineate the nuanced contours of facial matrices [20].

The complexities of craniofacial morphology are underpinned by a multifaceted interplay of hormonal, genetic, and epigenetic factors, including age, sex, population affinity, and environmental stimuli [21–29], which collectively create variability within and across populations. While historical research in craniofacial studies has predominantly aimed at discerning the genetic determinants of craniofacial variation, recent studies have pivoted towards identifying the biological origins of normative facial variability. Population affinity exerts a discernible influence on facial morphology, manifesting through ancestral imprints discernible within modern descendant groups, thereby outlining the morphological distinctions between and within populations. Furthermore, sexual dimorphism in craniofacial morphology, alongside alterations in size and shape during ontogenetic growth, underscores the intricate interplay of developmental dynamics [30].

The imperative to comprehend facial morphology across heterogeneous populations underscores its pivotal role in enhancing CFR methodologies, as the uniqueness inherent within each population group demands tailored approaches. In this context, the present study delves into the nuanced influences of population affinity, sex, age, and allometry on the variation and covariation of facial morphology matrices, meticulously studying French and white South African samples. Employing 3D reconstructions of CBCT scans and GMM analyses, this study attempts to outline the intricate interplay of biological and environmental factors in shaping craniofacial diversity. In this study, sex is defined as a set of biological characteristics related with physical as well as physiological features (for example, chromosomal genotype, hormone levels, internal and exterior anatomy).

2. Materials and methods

2.1. Materials

The study included 76 and 108 adult CBCT scans of white South Africans (29 males and 47 females) and French nationals (54 males and 54 females), respectively. The South African scans were collected retrospectively from the University of Pretoria's Oral and Dental Hospital and Groenkloof Life Hospital. The CBCT scans of the French nationals were acquired from the University of Bordeaux (France). Ethical approval was obtained from the Research Ethics Committee of the Faculty of Health Sciences at the University of Pretoria (Ethics Reference No. 222/2022). Existing scans were used to eliminate unnecessary exposure to radiation [31]. The white South Africans, ranging in age from 18 to 80 years (mean: 45.6, standard deviation: 20.0), were categorized into four age groups: 18–29 years, 30–44 years, 45–59 years, and 60+ years (Table 1). In contrast, the French nationals, aged between 18 and 60 years (mean: 37.5, standard deviation: 14.3), were divided into three age groups: 18–29 years, 30–44 years, and 45–59 years (Table 2). All patient data were anonymized, with the biological information relevant to the current investigation (sex, age, and population affinity) collected for analysis. We excluded scans of patients undergoing orthodontic treatment and those with pathological diseases, facial asymmetry, and any facial interventional reconstructive surgery to standardize the sample for uniformity. In this study, white South Africans were referred to as Africans (AFR) and French nationals as Europeans (EUR).

2.2. Methods

The CBCT scans were imported into the MeVisLab© v 2.7.1 program to extract volumetric data and for 3D image reconstruction. This GMM study used automated landmarks and 3D images to gather information on the morphology of hard and soft tissue facial matrices. Using the quantitative iterative thresholding method "Half Maximum Height" [32], threshold values between segmented elements were established to delineate hard and soft tissue surfaces.

For 3D image reconstruction, MeVisLab© v 2.7.1 interpolated intervals between each slice based on a defined grey threshold. The observer chose the depiction of tissues (hard or soft) through threshold segmentation, determined by selecting grey value intervals. Following segmentation, 3D surface meshes were generated and saved in ply format to create a 3D representation of the object [33]. In this study, the facial skeleton represented the hard tissue, while the exterior facial features represented soft tissue. Hard and soft tissue matrices were established by placing landmarks on the 3D reconstructions to analyze shape variation. To ensure homology and comparability between studies, we used classic definitions of craniometric and capulometric landmarks (types I, II, and III) [6,34–37]. Sliding landmarks aided the clear visualization of curved structures and the assessment of shape variations [34]. Using biological landmarks ensured that each identified point was the same on all surfaces in the sample [34]. A total of 652 landmarks—43 craniometric, 50 capulometric, and 559 sliding—were employed, as detailed in Tables S1, S2, and S3 and represented in Figs. 1, 2, and 3.

Of the 43 craniometric hard tissue landmarks, there were 19 bilateral pairs and five median landmarks (Table S1). Furthermore, each of the 559 hard tissue sliding landmarks (Table S2) was analyzed individually [38]. On the soft tissue, 50 capulometric landmarks were recorded: 31 bilateral pairs and seven median landmarks (Table S3). The hard tissue regions of interest included the midfacial matrix, further divided into the left and right orbits, left and right nasal bones, anterior nasal aperture, left and right zygoma, and left and right maxillae (Fig. 1). The soft tissue regions of interest included the facial features, mainly the eyes, ears, nose, and mouth (Fig. 2). The regions of interest for the hard-tissue sliding matrices were indicated along the exterior curves of the left and right external auditory meatuses (EAMs), which represented the left and right ears, the left and right orbits, which represented the eyes, and the anterior nasal aperture, which represented the nose (Fig. 3). The accuracy of the GMM analysis was enhanced by ensuring that each curve had the same number of landmarks along the curve and that all curves started at the same place. An existing craniometric landmark was

Table 1
Breakdown of white South African sample according to sex and age group.

Age group	Males	Females	n
18–29 years	7	13	20
30–44 years	9	9	18
45–59 years	6	15	21
60+ years	7	10	17
n	29	47	76

Table 2
Breakdown of French sample according to sex and age group.

Age group	Males	Females	*n*
18–29 years	10	19	29
30–44 years	40	24	64
45–59 years	4	11	15
n	54	54	108

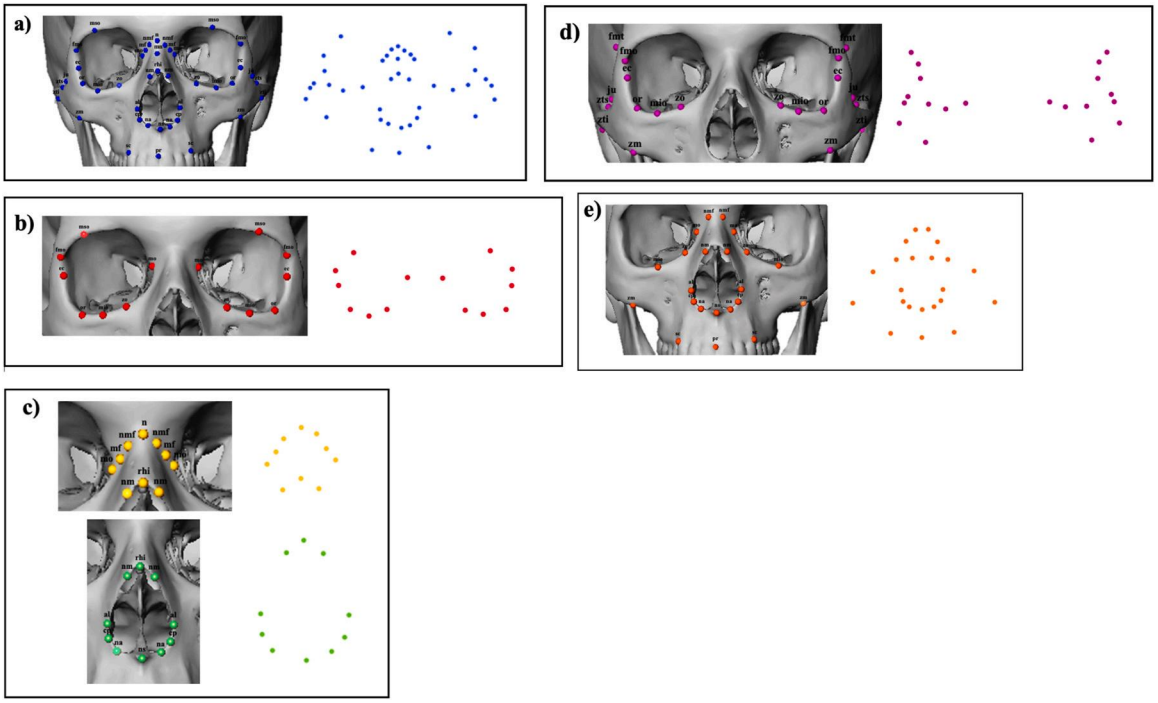

Fig. 1. Hard tissue region of interest: a) midfacial matrix, b) orbits, c) nasal bones and aperture, d) zygoma, and e) maxilla.

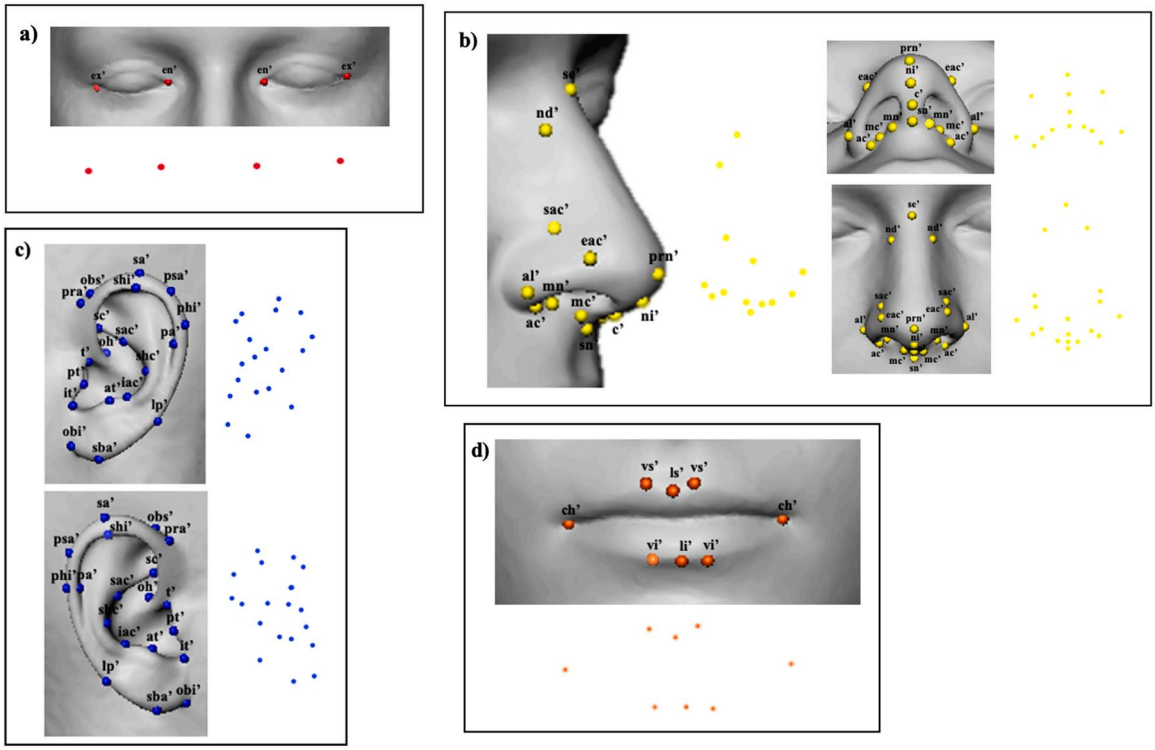

Fig. 2. Soft tissue region of interest: a) eyes, b) external nose, c) left (top) and right (bottom) ears, and d) mouth.

selected as the starting point for each sliding matrix (Table S2).

2.3. Alignment

The Frankfurt Horizontal (FH) plane was used to position landmarks on the hard tissue surfaces of the skulls. This plane, observable only on dry skulls or hard tissue representations, refers to three osteometric points: the right and left porion and the left orbitale [39]. For soft tissue surfaces, scans were oriented in the natural head position (NHP), where the tragus replaced the porion and the soft tissue orbitale acted as the anterior endpoint [40]. Given the repeatability of the NHP, landmarks were consistently positioned throughout the study [40,41].

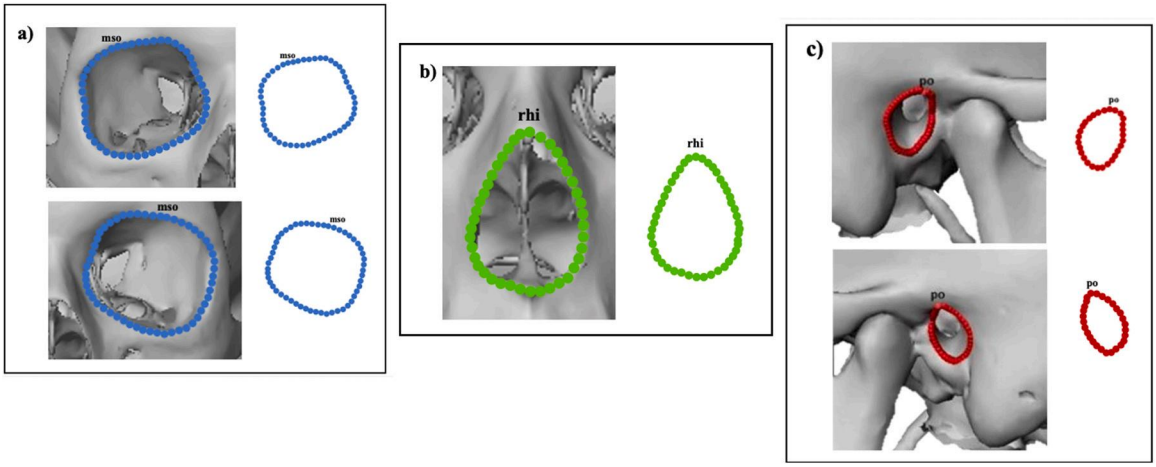

Fig. 3. Hard-tissue sliding matrices: a) left (top) and right (bottom) orbits, b) anterior nasal aperture, and c) left (top) and right (bottom) external auditory meatuses.

2.4. Automatic landmarking

Claes and colleagues [17] introduced the non-rigid registration method used in this study. The automatic landmarking method has recently been tested and validated by Ridel and colleagues [28,29,42] on facial hard and soft tissues and postcranial elements [43]. Automatic landmark placement is accurate and is an essential requirement for GMM to properly extract and assess anatomical areas from 3D models [19,28,42]. Fig. 4 depicts an adapted workflow of the automatic landmarking method [17,29,36].

2.5. Statistical analysis

Firstly, the reproducibility of 43 craniometric, 50 capulometric, and 559 sliding landmarks was assessed by examining landmark dispersion and comparing the dispersion to previous studies [6]. We measured dispersion for each landmark and individual as the average distance between a landmark's mean placement and subsequent placements. Reproducibility was determined using dispersion Δij for each landmark i and individual j, representing the mean Euclidean distance (MED) between landmarks i for all observations k (inter, intra, resp.) for subject j:

$$\Delta_{ij} = \sum_{k=1}^{K} \frac{\left\| p_{ijk} - \underline{p}_{ij} \right\|}{K}, \text{ with } \underline{p}_{ij} = \sum_{k=1}^{K} \frac{p_{ijk}}{K}$$

The reproducibility of automatically placed landmarks was evaluated by comparing interobserver errors (INTRA-OE) and interobserver errors (INTER-OE) between automatic and manual landmarking. Manual landmark placements were performed on MeVisLab© v 2.7.1, and ten scans from the entire sample were randomly selected to assess reproducibility.

According to previous research [44,45] on similar matrices and populations as those examined in this current study, the automatic placement of anatomical and sliding landmarks was effective between observers for all matrices and mostly resulted in lower dispersion errors.

A generalized Procrustes analysis (GPA) was performed on the raw landmark coordinates to produce orientation-invariant shape coordinates [46-48]. Raw landmark coordinates include information on the shape and size of the landmark, as well as "nuisance parameters" (orientation and position). By translating and scaling all landmark configurations to the same centroid size, and iteratively rotating all configurations until the summed squared distances between landmarks

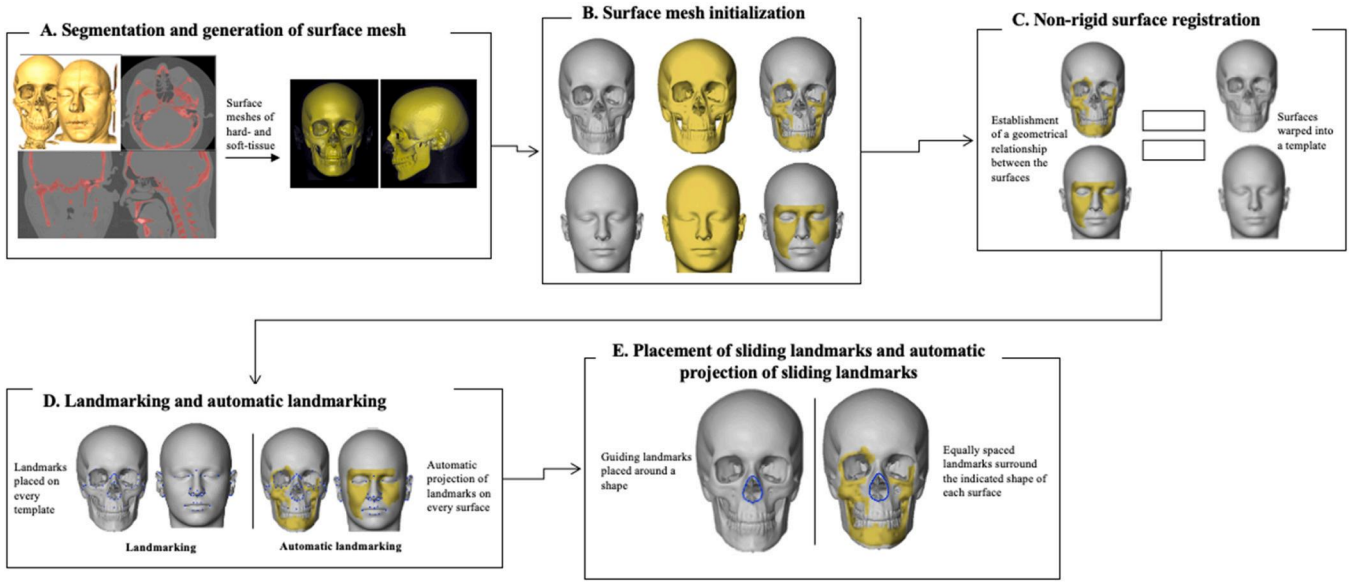

Fig. 4. Automatic landmarking. A. Segmentation and generation of surface mesh B. Surface mesh initialization C. Non-rigid surface registration D. Landmarking and automatic landmarking E. Placement of sliding landmarks and automatic projection of sliding landmarks.

and their corresponding sample average is a minimum [49–51], GPA separates shape from "nuisance parameters". The resultant superimposed, scaled, and rotated landmark configurations that arise are known as Procrustes shape coordinates, as they solely carry information about the shape of the configurations.

Principal component analysis (PCA) was used to derive principal component (PC) scores with maximum variance and covariation [46]. PC scores representing 95 % of the sample's overall variance were used for statistical analysis. The data was translated into a new coordinate system in which the first PC has the largest variation, and the second PC has the second greatest variance [52]. Individual observations were plotted along the PCA axes, which summarized variation in decreasing order. The projection of the data on that axis matched to the score of a given observation on that axis. As a result, each axis was a linear combination of the original observation variables [52]. Variable space was reduced to dimensions that express maximal variation by studying variation on the initial axes.

The distribution of hard and soft tissue PC scores was visualized using Q-Q plots [53]. Results were verified using non-parametric testing and considered reliable if both tests produced similar results. Landmark coordinates derived from the automatic landmarking were used to quantify and visualize the effects of population affinity variation, sexual dimorphism, and age differences on hard and soft tissue facial matrices, and independently tested the influence of sex and age on each population group to identify any population-specific differences.

Both parametric (MANOVA and MANCOVA) and non-parametric (50–50 MANOVA and permutation testing) tests were used to examine the significance of population affinity variation, sexual dimorphism, and age effects. Multiple analysis of variance (MANOVA) considers multiple continuous variables to determine if an independent variable, such as sex or age, significantly influences the dependent variable (shape variation). 50–50 MANOVA is a variant of MANOVA used for correlated response variables. Multiple analysis of covariance (MANCOVA) adjusts group means at follow-up to baseline differences while reducing within-group variance by removing covariate variation. Permutation testing involved comparing a chosen factor such as population affinity, age, or sex to sample values, with the null hypothesis rejected if the value fell within the random grouping range [36]. Each permutation test was repeated 10,000 times. For sex and population affinity classification, discriminant function analysis (DFA) was used with accuracies assessed through leave-one-out cross-validation [54], identifying linear combinations of variables with intergroup differences.

Allometry, the statistical relationship between size and shape, is crucial for understanding group form and shape differences, particularly in relation to sexual dimorphism [36,55,56]. Allometry was examined using PC scores from the sexual dimorphism study to generate linear models (hard and soft tissue shape vs. sex and centroid size). Pillai trace was used to examine the significance of each variable using MANCOVA (parametric) and 50–50 MANOVA (non-parametric), with size measured independently for each age group. The covariation between the hard tissue elements and the external soft tissue of the face of each sample was assessed using two-blocks partial least squares (PLS) analyses [57].

All statistical analyses for this study were performed using R-Studio 1.0.44-®2009–2016 for Windows [58], using the R-packages Morpho [59], Geomorph [60], and ffmanova [61,62].

3. Results

3.1. Reproducibility testing

For the AFR group, overall average landmark displacement errors for each matrix were less than 2 mm, except for the left orbit, which was less than 3 mm (Table S4). Regarding soft tissue configurations, for INTRA-OE, the eye exhibited the lowest dispersion (mean [M]: 0.433 mm; standard deviation [SD]: 0.028). The mouth had the lowest dispersion error for INTER-OE (M: 1.130 mm; SD: 0.519). The left ear had the highest dispersion error for INTRA-OE (M: 0.980 mm; SD: 0.381), and the right ear displayed the highest INTER-OE (M: 1.689 mm; SD: 0.802). Across all repeatability tests for hard tissue matrices, the left orbit had the largest dispersion errors, with mean values of 2.146 mm (SD: 0.075) and 1.592 mm (SD: 0.075) for INTRA-OE and INTER-OE, respectively. For INTER-OE, the left EAM exhibited the lowest dispersion error, with a mean value of 0.036 mm (SD: 0.196). For INTRA-OE, the anterior nasal aperture had the lowest mean dispersion error, with a mean value of 0.323 mm (SD:0.122).

In the EUR group, the mean dispersion error for all capulometric landmarks was less than 1 mm for INTRA-OE and INTER-OE (Table S5). For both INTER-OE and INTRA-OE, the mean dispersion error for craniometric and sliding landmarks on the hard tissue matrices was less than 2 mm. The right ear had the most variation among soft tissue matrices for both INTER-OE (M 1.034 mm; SD 0.220) and INTRA-OE (M: 0.900 mm; SD: 0.252). The eyes showed the lowest dispersion error for INTRA-OE with a mean value of 0.391 mm (SD: 0.050), while the mouth had the lowest INTER-OE (M: 0.465 mm; SD: 0.151). The INTER-OE and INTRA-OE of the craniometric landmarks on the midfacial matrix were similar, with a mean value of 0.990 mm (SD: 0.137), with the INTRA-OE being slightly lower than INTER-OE. In terms of hard tissue sliding landmarks (Table S5), the anterior nasal aperture had the lowest measurement errors for both INTER-OE (M: 0.376 mm; SD: 0.053) and INTRA-OE (M: 0.707 mm; SD: 0.058), with the INTER-OE being lower than INTRA-OE. The left orbit displayed the largest variability for both INTER-OE (M: 3.362 mm; SD: 2.061) and INTRA-OE (M: 3.261 mm; SD: 2.153) regarding hard tissue configurations.

Overall, the automatic placement of anatomical and sliding landmarks mostly resulted in lower dispersion mean ($\mu\ \Delta$) values.

3.2. Multivariate normality testing

Multivariate normality testing assessed whether PC scores were normally distributed [53], revealing an ideal distribution against real-squared Mahalanobis distances, with values close to the ideal diagonal.

For the whole sample combined, PC scores for the left and right ears showed some deviation from normality (Figure S1). PC scores for the hard-tissue right EAM showed minor deviation from normality, and the hard-tissue left EAM showed some divergence from normality (Figure S3). The PC score for the mouth (Figure S2), midfacial matrix (Figure S3), and eyes (Figure S1) showed only slight variations from normality. The PC score for the nose (Figure S2), anterior nasal aperture and left and right orbits (Figure S4) displayed some deviation from normality.

For the AFR sample, the PC scores for the left and right ears (Figure S5) displayed some deviation from normality. In contrast, minimal deviation from the normality was observed for the left and right EAMs (Figure S7). Some deviation from normality was observed for the eyes (Figure S5). mouth (Figure S6) and midfacial matrix (Figure S7). Additionally, there was some deviation from normality in the nose (Figure S6), left orbit, anterior nasal aperture (Figure S8).The right orbit, however, displayed a more pronounced deviation from normality (Figure S8).

In the EUR sample, there was minimal deviation from normality for the left ear, some deviation from normality for the right ear (Figure S9), and minimal deviation from normality for the left EAM and right EAMs (Figure S11). The mouth (Figure S10) and midfacial matrix (Figure S11) exhibited only slight deviations from normality; however, the eyes showed some divergence from normality (Figure S9). The nose (Figure S10), and left orbit (Figure S12) displayed some deviation from normality, although the anterior nasal aperture and right orbit only deviated slightly from normality (Figure S12).

3.3. Shape analysis of the hard and soft tissue matrices

Influence of population affinity on matrix shape: According to both parametric (MANOVA) and non-parametric (permutation testing and 50–50 MANOVA) analyses, significant differences in population affinity between the AFR and EUR groups influenced both hard and soft tissue matrices ($p < 0.05$) (Table 3).

When assessing soft tissue configurations, the mouth had the lowest classification accuracy (69 %), while the left ear, right ear, eyes, and nose had classification accuracies above 80 % (Table 3). No statistical difference was observed for the ears (Fig. 5) and eyes (Fig. 6); however, the scatterplots of the two populations overlapped significantly. The two population groups did not show any significant overlap or distinct separation for the nose, and no grouping of the two populations was observed for the mouth (Fig. 6).

Covariation between population affinity and size was not significant for ears, with size not influencing the shape of the ears (Table 3). However, covariation between population affinity and age and covariation between population affinity and sex were found to be significant for both the left and right ears (Table 3). Additionally, we observed that size did not affect the morphology of the eyes when considering population affinity. However, population affinity covaried significantly with sex and age for the eyes (Table 3). Population affinity covaried significantly with size, age, and sex for the nose (Table 3). When the relationship to population affinity was evaluated, size and age did not affect variation in mouth shape, but sex had a statistical impact on the shape of the mouth (Table 3).

When hard tissue shape configurations were assessed, all classification accuracies were above 80 %, except for the left orbit, which had the lowest accuracy (71 %). The left EAM had the highest accuracy (100 %), indicating that all individuals in the sample were correctly classified. The scatterplots of the midfacial matrix overlapped considerably and could not clearly distinguish between the two populations (Fig. 7).

For the midfacial matrix, there was no significant covariation between population affinity and size (Table 3), indicating that size has no effect on the form of the midfacial matrix. However, population affinity covaried significantly with age and sex for the midfacial matrix (Table 3), indicating that age and sex have an influence on the morphology of the midfacial matrix.

For the left EAM, the population groups varied significantly; however, for the right EAM, there was no statistical separation between populations (Fig. 7). Population affinity covaried significantly with size, age, and sex for both the left and right EAMs (Table 3), indicating that these variables have an effect on the form of the left and right EAMs. There was no distinct separation between the populations in terms of the left or right orbits (Fig. 8). Population affinity did not covary significantly with size for the left and right orbits; however, population affinity covaried with age and sex for the left and right orbits (Table 3).

For the anterior nasal aperture, no clear separation with minor overlapping was observed between populations (Fig. 8). Population affinity did not covary significantly with size for the anterior nasal aperture; however, population affinity covaried significantly with age and sex (Table 3).

Population differences had a substantial impact on both hard and soft tissue matrices; however, overlap existed between the two population groups on all PCA graphs.

Influence of sexual dimorphism on matrix shape: To understand sexual dimorphism in the two populations, we examined the effect of sex on facial matrix shape for the complete sample and for each population group separately.

In soft tissue matrices, using both parametric (MANOVA and MANCOVA) and non-parametric (permutation testing and 50–50 MANOVA) tests sex significantly influenced mouth shape in the AFR group (Table 4), but there was no notable separation between sexes on PCA (Fig. 9). In the EUR group, sex significantly influenced the shape of the ears, nose, and mouth (Table 4), with minor overlap observed between the sexes (Figs. 9 and 10).

In hard tissue matrices, sex significantly influenced the shape of the midfacial matrix and left EAM in the AFR group (Table 4) with no separation observed between sexes for both the midfacial matrix and left EAM; however, minor overlapping was observed for both matrices (Fig. 11). In the EUR group, sex significantly influenced the shape of the midfacial matrix, right EAM, right orbit, and anterior nasal aperture (Table 4), with no clear separation between sexes observed for the midfacial matrix, right EAM, right orbit, and anterior nasal aperture (Figs. 12 and 13).

When both soft and hard tissue shape configurations were assessed, none of these matrices could be classified into male or female categories with an accuracy above 80 %, except for the left EAM in the AFR group, which achieved a classification accuracy of 95 % (Table 4). The classification accuracy for sex mostly ranged between 60 % and 70 %. In contrast to the AFR group, classification accuracy was generally greater in the EUR group (Table 4).

Regarding covariation in the whole sample, sex covaried significantly with population affinity for the right ear and nose (Table 4). In terms of hard tissue, sex covaried significantly with population affinity for the midfacial matrix, right EAM, left orbit, and right orbit (Table 4).

For the soft tissue matrices, in the AFR group, sex covaried significantly with size for nose shape, while in the EUR group, sex did not covary with size.

For the hard tissue matrices, in the AFR group, sex covaried significantly with size for the left EAM (Table 4). In the EUR group, sex did not

Table 3
Hard and soft tissue population differences.

		Population differences					Covariates		
							Pop*Size	Pop*Age	Pop*Sex
		Test[1]	Test[2]	Test[3]	DFA	Group PCA	Test[3]		
Soft-tissue	Left ear	**0.001** **	**0.001**	**2.180e−10** ***	86 %	91 %	0.695	**2.430e−08** ***	**1.020e−11** ***
	Right ear	**0.001** **	**0.001**	**2.890e−14** ***	91 %	94 %	0.905	**1.990e−11** ***	**<2e−16** ***
	Eyes	**0.001** **	**0.001**	**<2e−16** ***	86 %	85 %	0.703	**<2e−16** ***	**<2e−16** ***
	Nose	**0.001** **	**0.001**	**<2e−16** ***	97 %	73 %	**0.001** **	**<2e−16** ***	**<2e−16** ***
	Mouth	**0.011** *	**0.010**	**0.015** *	69 %	75 %	0.140	0.078	**0.001****
Hard-tissue	Midfacial matrix	**0.001** **	**0.001**	**<2e−16** ***	96 %	99 %	0.091.	**<2e−16** ***	**<2e−16** ***
	Left EAM	**0.001** **	**0.001**	**<2e−16** ***	100 %	100 %	**3.360e−05** ***	**<2e−16** ***	**<2e−16** ***
	Right EAM	**0.001** **	**0.001**	**2.380e−08** ***	82 %	78 %	**0.019** *	**3.780e−05** ***	**6.720e−12** ***
	Left orbit	**0.003** **	**0.001**	**3.350e−4*****	71 %	81 %	0.322	**0.011***	**2.040e−4** ***
	Right orbit	**0.001** **	**0.001**	**7.190e−16** ***	87 %	83 %	0.121	**9.700e−13** ***	**<2e−16** ***
	Nasal aperture	**0.001** **	**0.001**	**<2e−16** ***	94 %	93 %	0.389	**<2e−16** ***	**<2e−16** ***

Test[1]= MANOVA, Test[2]= Permutation testing, Test[3]= 50–50 MANOVA. Significant p-value (<0.05) are indicated in bold. **= p-values less that 0.01 and *** = p-values less than 0.001. EAM, external auditory meatus

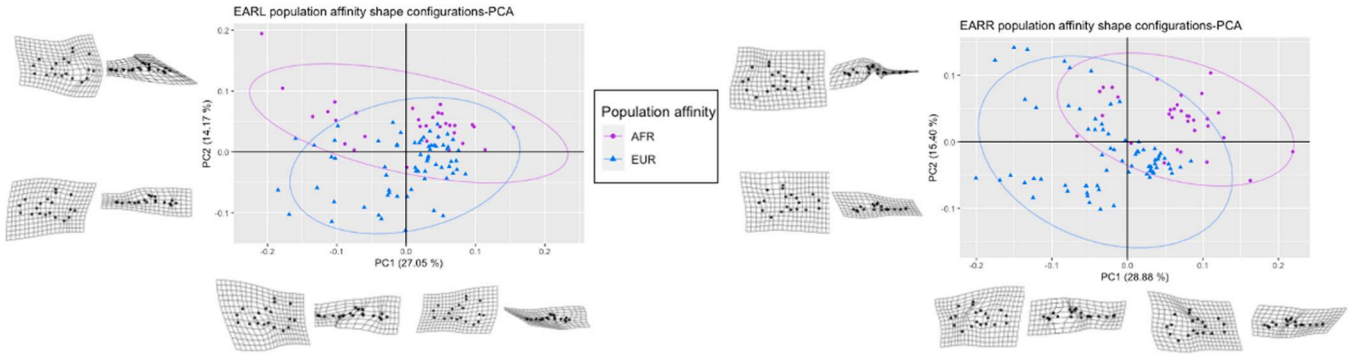

Fig. 5. PC 1 versus PC 2 of the complete sample for population affinity indicating the maximum and minimum of the shapes of the soft tissue left (left) and right (right) ears along PC1. AFR = white South African sample; EUR = French sample.

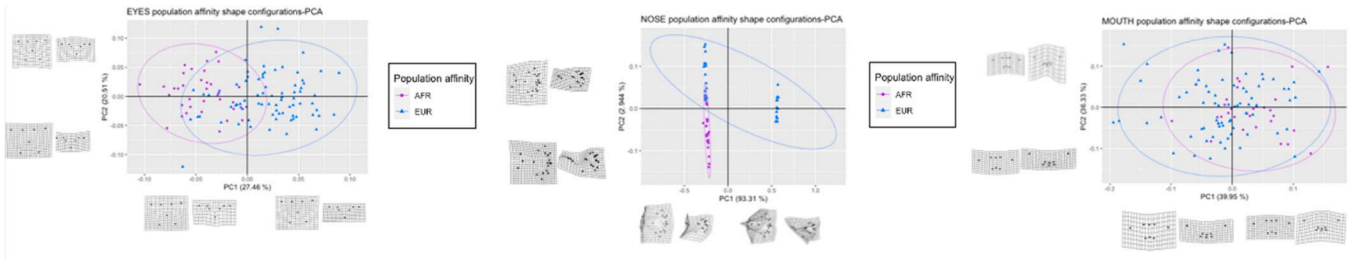

Fig. 6. PC 1 versus PC 2 of the complete sample for population affinity indicating the maximum and minimum of the shapes of the soft tissue eyes (left), nose (middle) and mouth (right) along PC1. AFR = white South African sample; EUR = French sample.

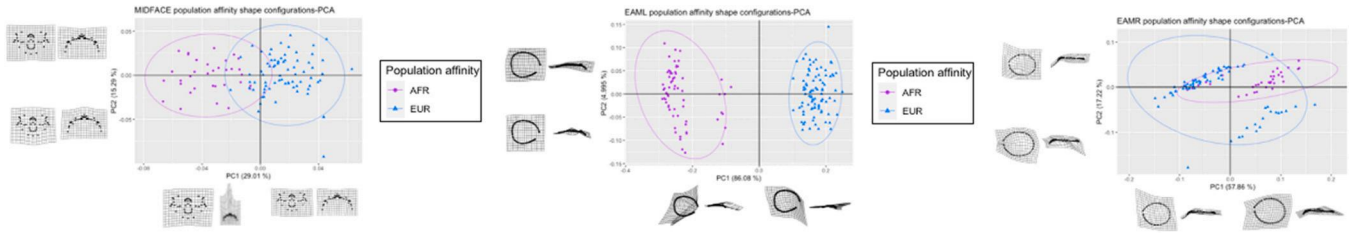

Fig. 7. PC 1 versus PC 2 of the complete sample for population affinity indicating the maximum and minimum of the shapes of the hard-tissue midfacial matrix (left), left EAM (middle) and right EAM (right) along PC1. AFR = white South African sample; EUR = French sample.

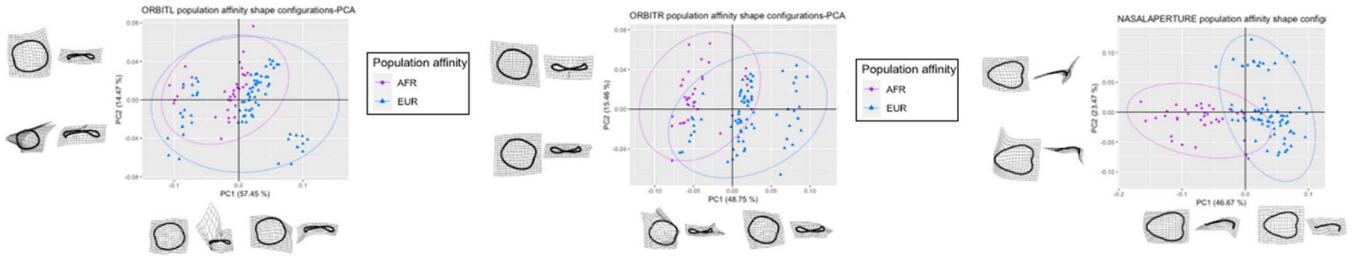

Fig. 8. PC 1 versus PC 2 of the complete sample for population affinity indicating the maximum and minimum of the shapes of the hard-tissue left orbit (left), right orbit (middle) and anterior nasal aperture (right) along PC1. AFR = white South African sample; EUR = French sample.

covary significantly with size for any of the hard tissue matrices (Table 4).

Influence of age on matrix shape: Using parametric (MANCOVA) and non-parametric (50–50 MANOVA) tests, for the whole sample, only eye shape varied with age (Table 5). In the AFR group, age significantly influenced the shape of the left EAM and left orbit (Table 5), with no separation by age observed for the left EAM and left orbit (Fig. 14). In the EUR group, age had a significant influence on the shape of the left ear, eyes, and external nose (Table 5), with no separation observed for the left ear, eyes, and nose (Fig. 15).

For the whole sample, age covaried significantly with population affinity for all the soft and hard tissue matrices except the mouth (Table 5). Additionally, age covaried significantly with both population affinity and sex for all soft and hard tissue matrices (Table 5). Age co-varied significantly with sex only for the right ear, the midfacial matrix, and left EAM.

For the AFR group, age covaried significantly with sex for mouth shape, the left EAM, and the left orbit, whereas in the EUR group, all soft

Table 4
Hard and soft tissue sexual dimorphism in the complete sample and within each population.

		Complete sample		White South African						French				
		Covariates Pop*Sex		Test[1]	Test[2]	Test[3]	Test[4]	DFA	Group PCA	Covariates Size*sex Test[3]	Test[1]	Test[2]	Test[3]	Test[4]	DFA	Group PCA	Covariates Size*sex Test[3]
		Test[3]	Test[4]														
Soft-tissue	Left ear	0.131	0.131	0.195	0.202	0.289	0.289	66 %	56 %	0.910	**0.001** **	**0.001**	**4.950e−06** ***	**4.953e−06** ***	80 %	82 %	0.513
	Right ear	**1.869e−4*** **	**1.869e−4** ***	0.356	0.361	0.468	0.468	63 %	56 %	0.757	**0.001** **	**0.001**	**1.410e−05** ***	**1.407e−05** ***	73 %	77 %	0.598
	Eyes	0.561	0.5614	0.133	0.154	0.085.	0.085	67 %	61 %	0.111	0.249	0.246	0.217	0.217	61 %	59 %	0.210
	Nose	**3.243e−4*** **	**3.239e−4*** **	0.968	0.960	0.960	0.960	68 %	72 %	**2.860e−4** ***	**0.001** **	**0.001**	**2.120e−07** ***	**2.116e−07** ***	79 %	85 %	0.112
	Mouth	0.142	0.142	**0.021*** *	**0.027**	**0.024***	**0.024***	69 %	59 %	0.181	**0.014** *	**0.014**	**0.015** *	**0.015** *	74 %	64 %	0.059
Hard-tissue	Midfacial matrix	**0.001*** **	**9.890e−4** ***	**0.013** *	**0.018**	**0.013** *	**1.297e−2***	71 %	74 %	0.232	**0.002** **	**0.003**	**5.280e−3** **	**5.281e−3** **	68 %	66 %	0.973
	Left EAM	0.277	0.277	**0.001** **	**0.001**	**<2e−16** ***	**<2.2e−16** ***	95 %	94 %	**4.240e−3** **	0.960	0.953	0.956	0.956	62 %	51 %	0.677
	Right EAM	**0.001****	**1.079e−3** **	0.456	0.454	0.211	0.211	66 %	51 %	0.804	**0.007** **	**0.006**	**3.080e−05** ***	**3.083e−05** ***	74 %	69 %	0.579
	Left orbit	**0.021***	**2.074e−2** *	0.327	0.289	0.161	0.161	63 %	66 %	0.357	0.034 *	0.052	0.063	0.063.	72 %	69 %	0.432
	Right orbit	**0.009****	**9.728e−3** **	0.573	0.581	0.471	0.471	60 %	46 %	0.877	**0.003** **	**0.001**	**2.670e−05** ***	**2.674e−05** ***	72 %	69 %	0.200
	Nasal aperture	0.120	0.119	0.931	0.932	0.926	0.926	60 %	34 %	0.558	**0.015** *	**0.019**	**0.0183** *	**1.827e−2** *	68 %	68 %	0.543

Test[1]= MANOVA, Test[2]= Permutation testing Test[3]= 50–50 MANOVA, Test[4]= MANCOVA. Significant p-values ($p < 0.05$) are indicated in bold; **= p-values less that 0.01 and *** = p-values less than 0.001. EAM, external auditory meatus

and hard tissue matrices, except the mouth, left EAM, left orbit, and anterior nasal aperture, were significantly influenced by the covariates age and sex (Table 5).

Influence of allometry on matrix shape*:* Allometry assesses the effect of size on shape and not size variation recorded for every individual in the sample. Based on MANCOVA and 50–50 MANOVA, for the whole sample, size alone influenced the shape of the eyes, nose, mouth, midfacial matrix, right EAM, left orbit, and right orbit (Table 6). Additionally, size covaried significantly with population affinity for the shape of the nose and the left and right EAMs. Size also covaried significantly with sex for the shape of the nose and the left EAM. Size, population affinity, and sex covaried significantly to influence the shape of the mouth and left EAM (Table 6).

In the AFR group, size did not influence any of the soft tissue matrices, while all hard tissue matrices showed significant variation, except the right orbit and anterior nasal aperture. Additionally, size only covaried with sex to influence the shape of the nose and left EAM (Table 6).

In the EUR group, for the soft tissue matrices, size significantly influenced eye and nose shape. All the hard tissue matrices except the left EAM and anterior nasal aperture were significantly influenced by size (Table 6). There was no covariation between size and sex for any of the soft and hard tissue matrices (Table 6).

3.4. Craniofacial variation that considers population affinity, sex, and age

We examined the impact of population affinity on soft tissue facial matrices**,** revealing that the AFR and EUR groups had varying left ear morphologies (Fig. 5). The AFR group predominantly had wider left ears than the EUR group, with some overlap indicating a small percentage of positively correlated individuals. Similarly, for the right ear, the EUR group had smaller right ears than the AFR group (Fig. 5). Regarding eye shape, the AFR group generally had smaller, narrower eyes, while the EUR group had wider or bigger eyes (Fig. 6). For the nose, the AFR group had the most significant nasal variances with a narrower and elongated shape (Fig. 6). The EUR group displayed minimal anatomical changes in nose shape. Both groups had similarly shaped mouths, but the EUR group exhibited significant variation, including a larger superior border and a thinner, smaller inferior border of the mouth (Fig. 6).

Concerning hard tissue shape changes, midfacial matrix morphology showed some overlap in both groups, with the EUR group having a larger, wider shape and the AFR group having a smaller, rounder shape (Fig. 7). Regarding left EAM shape, a smaller, narrower morphology was noted in the AFR group, while the EUR group had bigger, wider left EAMs (Fig. 7). Furthermore, the AFR group had the most pronounced changes in left EAM morphology than observed in the EUR group. Similar patterns to the left EAM were observed for anatomical changes in the right EAM (Fig. 7). The shape of the right EAM varied the most in the EUR group compared to the AFR group. The right EAM morphology was smaller in the EUR group and larger in the AFR group.

Regarding the shape of the left and right orbits, both groups had similar shape patterns (Fig. 8). The EUR group had significantly rounder and larger left orbits than the AFR group and slightly rounder and larger right orbits than the AFR group (Fig. 8). The anterior nasal aperture, particularly the nasion, had comparable shape patterns, but the EUR group had a slightly elongated and larger morphology than observed in the AFR group (Fig. 8).

Sexual dimorphism contributed to significant morphological changes in the mouth (Fig. 9), midfacial, and left EAM configurations in the AFR group (Fig. 11). Sexual dimorphism contributed to significant changes in both ears (Fig. 10), nose (Fig. 10), mouth (9), midfacial matrix (Fig. 12), right EAM (Fig. 12), right orbit (Fig. 13), and anterior nasal aperture (Fig. 13) in the EUR group. In the AFR group, males had wider mouths and larger and wider midfaces than females (Figs. 9, 11). Although females had the most variable left EAM shape, they had smaller, and

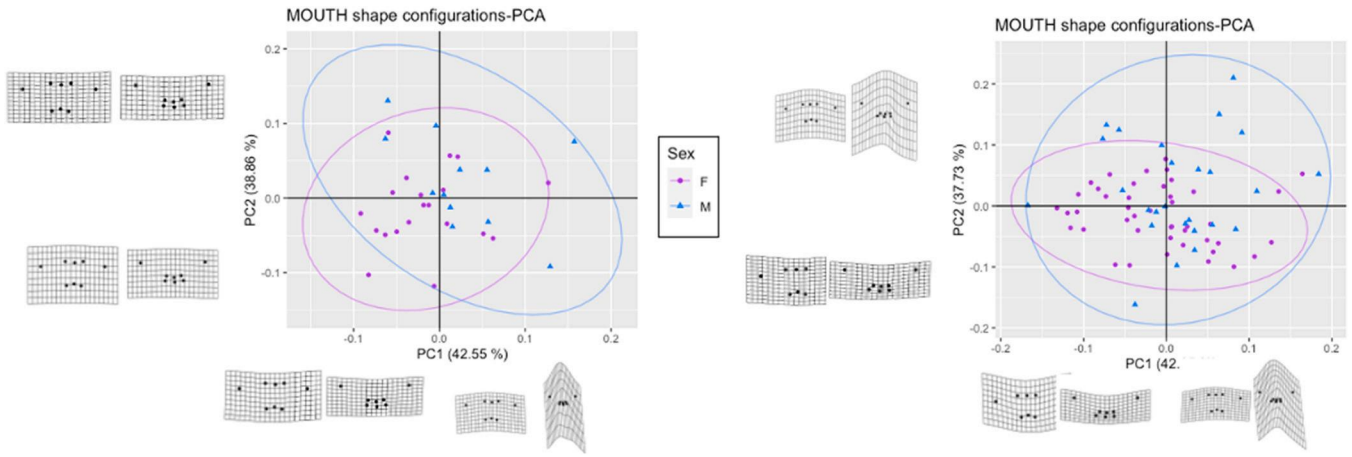

Fig. 9. PC 1 versus PC 2 for sex indicating the maximum and minimum of the shapes of the soft tissue mouth along PC1 for the white South African sample (AFR group) (left) and French sample (EUR group) (right). F = female; M = male.

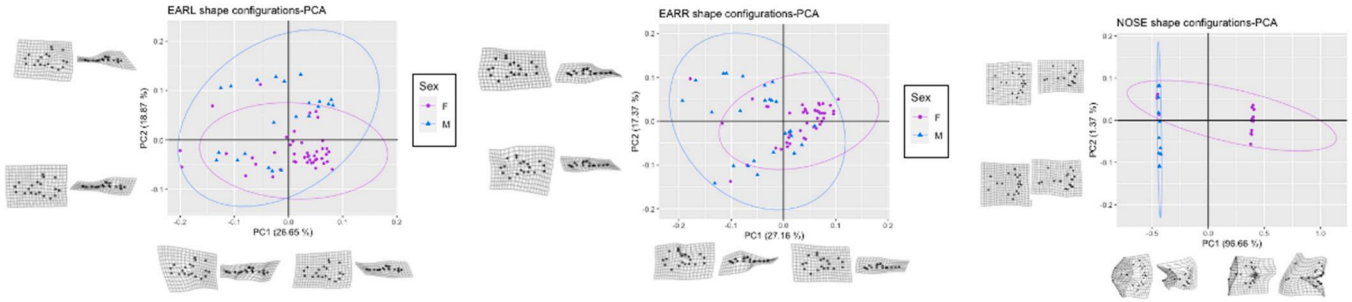

Fig. 10. PC 1 versus PC 2 of the French sample (EUR group) for sex indicating the maximum and minimum of the shapes of the soft tissue left ear (left), right ear (middle) and external nose (right) along PC1. F = female; M = male.

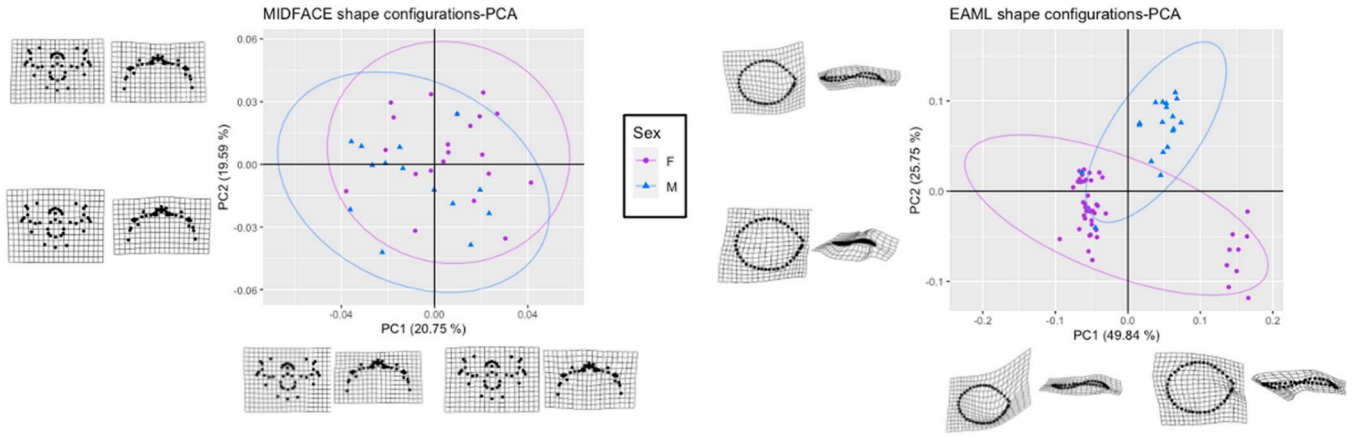

Fig. 11. PC 1 versus PC 2 of the white South African sample (AFR group) for sex indicating the maximum and minimum of the shapes of the hard-tissue midfacial matrix (left) and left EAM (right) along PC 1. F = female; M = male.

rounder left EAMs than males (Fig. 11).

In the EUR group, males and females had identically shaped ears, but the ears of the males were larger and more pronounced (Fig. 10). Males displayed the most variability in nose shape and had larger noses compared to females (Fig. 10). Females had considerably smaller, narrower, and extended noses, with the smallest changes in shape configuration (Fig. 10). Males had larger and wider mouths than females, whose mouths were smaller and thinner (Fig. 9). In the EUR group, males and females had comparable midfacial matrices (Fig. 12); however, females had a slightly smaller midfacial morphology. Males and females had similarly shaped right EAMs, with the most variation being observed among males, who had larger, and rounder left EAMs (Fig. 12). Males had larger and more circular orbital shapes than females (Fig. 13). Females had a smaller anterior nasal aperture shape than males, who had larger and slightly more elongated nasal aperture shapes than females (Fig. 13).

In the AFR group, the shape of the left EAM and left orbit changed significantly with age (Fig. 14). In the EUR group, the shape of the left ear, eyes, and nose changed significantly with age (Fig. 15). In the AFR group, the left EAM's smaller morphology was consistent across all age

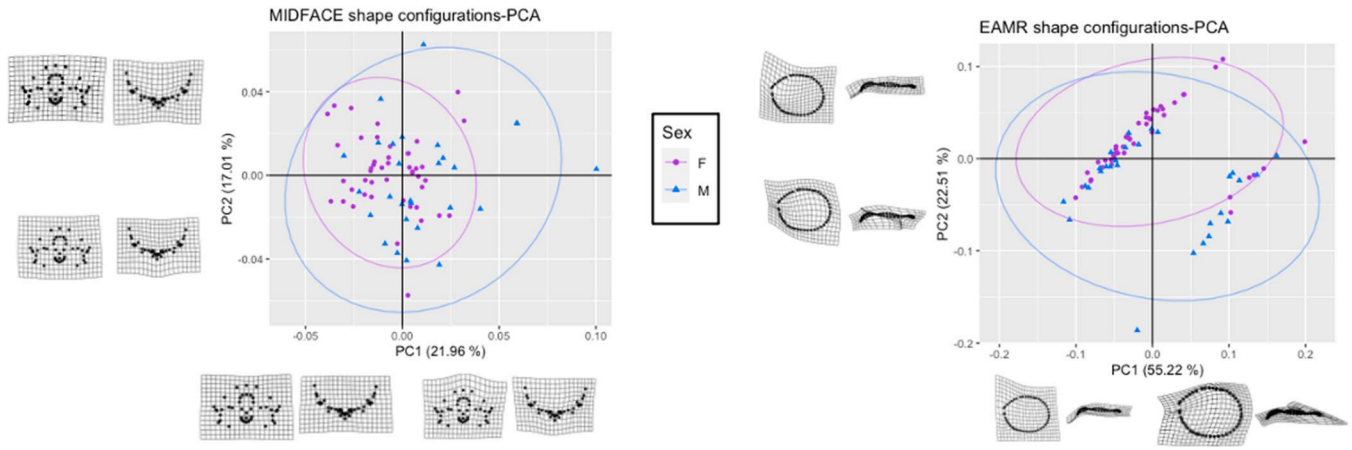

Fig. 12. PC 1 versus PC 2 of the French sample (EUR group) for sex indicating the maximum and minimum of the shapes of the hard-tissue midfacial matrix (left) and right EAM (right) along PC 1. F = female; M = male.

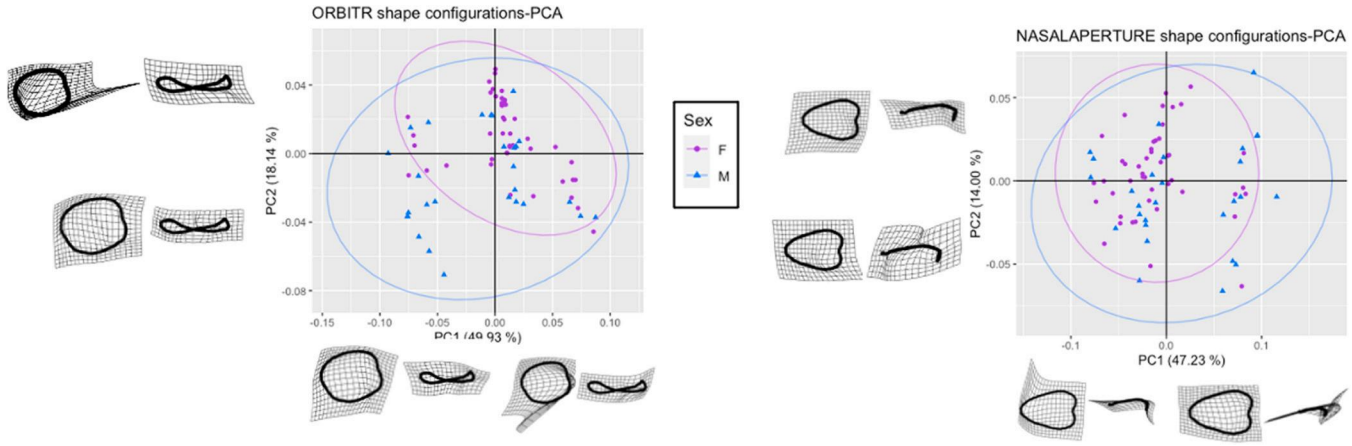

Fig. 13. PC 1 versus PC 2 of the complete French sample (EUR group) for sex indicating the maximum and minimum of the shapes of the hard-tissue right orbit (left) and anterior nasal aperture (right) along PC 1. F = female; M = male.

cohorts, as was the large and circular shape configuration of the left orbit (Fig. 14). The EUR group exhibited variation in the shape of the left ear at 30–44 years, with larger ears than other age cohorts (Fig. 15). Eye shape remained similar across all age groups, while differences in nose shape were prominent in the 30–44 years and 60+ years age groups, with a wider external shape (Fig. 15).

3.5. Correlations between hard and soft tissue facial matrices

All soft tissue matrices were positively correlated with the midfacial matrix in the EUR and AFR groups (Table 7). In the AFR group, the strongest correlations were observed between the shape of the midfacial matrix and left ear, followed by the midfacial matrix and the right ear, and the midfacial matrix and the nose. The eyes were moderately correlated to the shape of the midfacial matrix and had the weakest correlation to the midface. Additionally, the shapes of the left ear and right ear were strongly correlated to their corresponding EAMs. Furthermore, the shape of the nose was strongly correlated to the anterior nasal aperture in the AFR group. Correlations in the AFR group were all significant (p-value < 0.05) for all strong correlations, including the eyes (Table 7). In contrast, in the EUR group, all the correlations were weak but positive. The shape of the left ear and the right ear was correlated to its corresponding and differing EAM (Table 7). Furthermore, nose shape was moderately correlated to the anterior nasal aperture in the EUR group. Only the correlation between the right ear and right EAM was found to be significant.

4. Discussion

In our study, we investigated the influence of population affinity, sex, age, and allometry on the facial matrices of a sample of white South Africans and French nationals. We also tested whether the hard and soft tissue matrices were correlated. To account for laterality-specific variations, both the right and left parts of the hard and soft tissue facial matrices, such as the EAMs, orbits, eyes, and ears, were included.

4.1. Craniofacial shape variation that considers population affinity, sex, and age

Our analysis recognized the hierarchal structure of these factors, and we conducted the analysis in order of population affinity, then sex, age, and finally allometry [63]. Ritz-Timme et al. [64] emphasized that while facial features are present across populations, their frequencies vary. Our findings highlighted the important role of population affinity in shaping both hard and soft tissue morphology, demonstrating population-specific differences. Sexual dimorphism and aging were also influential factors within both populations.

The influence of population affinity on facial morphology is well known. We observed that white South Africans have larger and wider ears, whereas French people have smaller and narrower ears. Similarly,

Table 5
Hard and soft tissue shape change associated with age in the complete sample and within each population.

		Complete sample								White South African						French					
		Age		Pop*Age		Sex*Age		Pop*Sex*Age		Age		Sex*Age				Age		Sex*Age			
		Test[3]	Test[4]	Test[3]	Test[4]	Test[3]	Test[4]	Test[3]	Test[4]	Test[3]	Test[4]	Test[3]	Test[4]			Test[3]	Test[4]	Test[3]	Test[4]		
Soft-tissue	Left ear	0.064	0.069	**2.430e−08** ***	**2.366e−07** ***	0.239	0.248	**9.920e−08** ***	**7.269e−07** ***	0.423	0.439	0.635	0.562			**0.013***	**0.016***	**8.240e−07** ***	**1.305e−06** ***		
	Right ear	0.381	0.379	**1.990e−11** ***	**7.089e−09** ***	**0.031***	**0.050***	**1.120e−10** ***	**3.375e−09** ***	0.409	0.374	0.724	0.698			0.132	0.132	**1.390e−4** ***	**1.867e−4** ***		
	Eyes	**0.038***	**0.041***	**<2e−16** ***	**1.116e−11** ***	0.226	0.227	**1.090e−13** ***	**2.245e−08** ***	0.696	0.688	0.564	0.575			**5.670e−3** **	**5.429e−3** **	**0.032***	**0.028***		
	Nose	0.741	0.728	**<2e−16** ***	**3.101e−08** ***	**0.039***	0.056	**<2e−16** ***	**8.918e−11** ***	0.061	0.055	0.588	0.515			**2.820e−3** **	**0.010***	**2.980e−09** ***	**1.594e−06** ***		
	Mouth	0.157	0.149	0.078.	0.087.	0.090	0.082	**2.100e−05** ***	**2.570e−4** ***	0.476	0.474	**0.035***	**0.021***			0.139	0.144	0.139	0.144		
Hard-tissue	Midfacial matrix	0.265	0.265	**<2e−16** ***	**7.510e−15** ***	**4.200e−3** **	**4.034e−3** **	**<2e−16** ***	**1.010e−14** ***	0.632	0.608	0.173	0.194			0.192	0.183	**0.003****	**0.003****		
	Left EAM	0.100	0.099	**<2e−16** ***	**< 2.2e−16** ***	**3.560e−4***	**3.138e−4***	**<2e−16** ***	**< 2.2e−16** ***	**0.040***	**0.036***	**<2e−16** ***	**1.287e−10** ***			0.831	0.827	0.208	0.233		
	Right EAM	0.658	0.651	**3.780e−05** ***	**2.387e−4** ***	0.074	0.088.	**2.510e−07** ***	**1.186e−06** ***	0.098	0.122	0.234	0.200			0.869	0.866	**0.002****	**0.002****		
	Left orbit	0.530	0.518	**0.011***	**0.019***	0.172	0.172	**0.011***	**0.024***	**0.017***	**0.034***	**0.011***	**0.040***			0.677	0.662	0.270	0.258		
	Right orbit	0.868	0.864	**9.7e−13** ***	**1.183e−08** ***	0.125	0.144	**5.630e−13** ***	**2.829e−07** ***	0.262	0.290	0.343	0.403			0.434	0.422	**0.007****	**0.013***		
	Nasal aperture	0.637	0.626	**<2e−16** ***	**8.662e−16** ***	0.333	0.322	**<2e−16** ***	**2.424e−13** ***	0.230	0.201	0.430	0.374			0.431	0.431	0.205	0.199		

Test[3] = 50–50 MANOVA, Test[4] = MANCOVA. Significant p-values (p <0.05) are indicated in bold. **= p-values less that 0.01 and *** = p-values less than 0.001. EAM, external auditory meatus

white South Africans are observed to have larger left ears, while black South Africans have larger right ears [44], suggesting that ear shape can be used to differentiate between different populations. Sforza et al. [65], for example, observed that the ears of white Italians often increase in length rather than width. According to a different study evaluating variations in human ear shape, people from the Indian subcontinent have long ears, followed by Caucasians, while Afro-Caribbeans have the smallest ears [66]. Another study observed that Ashkenazi and Sephardi Jews have larger earlobes than Jews and Arabs in Israel [67]. In terms of soft tissue differences, we found that white South Africans have narrower, elongated noses than French people. Another South African study [28] reported that white South Africans had longer and more prominent external noses, which is consistent with our findings. Interestingly, a Chinese and European study [36] showed that the centroid sizes of soft tissue noses are similar across these populations, which is unexpected given their geographical backgrounds.

According to our findings, French people had wider midfacial matrices, while South Africans had smaller and rounder midfacial matrices. The French group also had larger and rounder EAMs. We found that both groups had comparable orbital and anterior nasal aperture shape patterns but that French people had larger and more rounded orbits and slightly longer and larger anterior nasal apertures. Erasmus et al. [44] observed that white South Africans had smaller right EAMs, whereas we observed larger right EAMs amongst white South Africans. Contrary to our findings, white South Africans are observed to have a pear-shaped nasal aperture contour [28,68].

Based on findings, facial shape variation is essentially distinct for each face, and the shape variety of both hard and soft tissue facial matrices implies morphological variances in both the face and facial skeleton. As a result of this variation, the samples were treated as distinct entities. The differences discovered across the two groups were expected given that the populations are influenced by different eco-geographical factors, and thus acclimatized to different environmental circumstances, resulting in diverse adaptations.

We observed sexual dimorphism in both population groups, specifically in the mouth, midfacial matrix, and left EAM of white South Africans and the ears, nose, mouth, midfacial matrix, right EAM, right orbit, and anterior nasal aperture of French people. Based on our findings, males have wider mouths, larger noses, and larger midfaces than females. These findings are consistent with Agbolade et al. [63], who observed that Irish and British males have larger mouths and noses than females. Contrary to our results, Farrera et al. [69] observed that Mexican males have shorter mouths than females, whereas larger noses were found in Mexicans males than females, which is similar to our findings. Similar to our findings Sforza et al. [65] reported that males have larger ears than females. Ridel et al. [28] also reported that white and black South African males had larger centroid sizes than males, demonstrating sexual dimorphism for both hard and soft tissue. Sexual dimorphism has also been reported for all hard and soft tissue matrices, excluding the inferior facial hard tissue matrix, in studies focusing on French people, however French females had wider ears than males [6], which is inconsistent with our findings. Erasmus et al. [44] reported that white South African males have more diverse ear shapes than females but that females have larger ears and EAMs, which is in contrast to our findings. The fact that sexual dimorphism is highly population specific may explain these discrepancies [30]. Sexual dimorphism varies between populations in terms of particular features and their expression; differences between males and females in a population may be less or more prominent than in a different population [70]. According to our findings and the aforementioned studies, adult male faces are generally larger.

In our study, age was associated with the variability of left ear and left orbit shape in white South Africans, whilst the shape of the left ear, eyes, and nose varied with age among French people. These findings are consistent with previous reports of hard and soft tissue shape changes across age cohorts. We found that individuals who were between 30 and

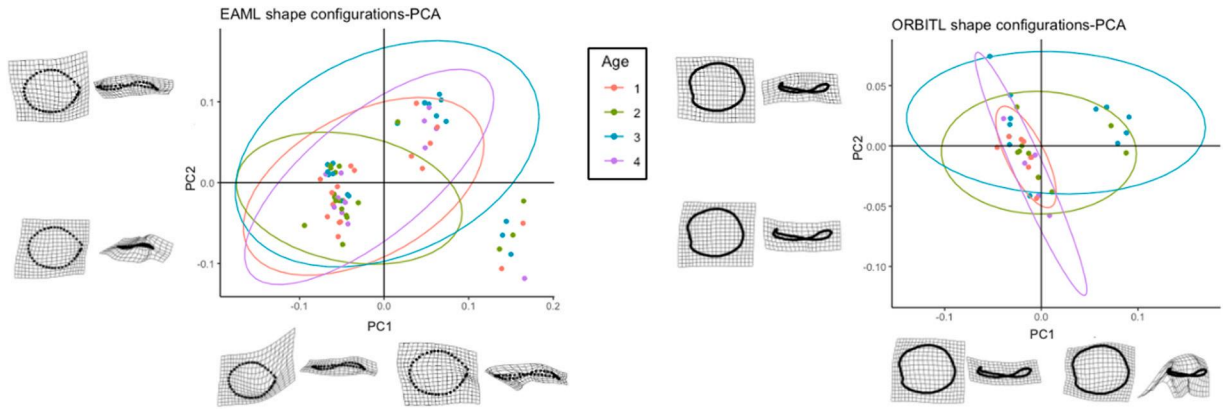

Fig. 14. PC 1 versus PC 2 of the white South African sample (AFR group) for age indicating the maximum and minimum of the shapes of the hard-tissue left external auditory meatus (EAM) (left) and left orbit (right) along PC 1. 1 = 18–29 years old; 2 = 30–44 years old; 3 = 45–59 years old; 4 = 60+ years.

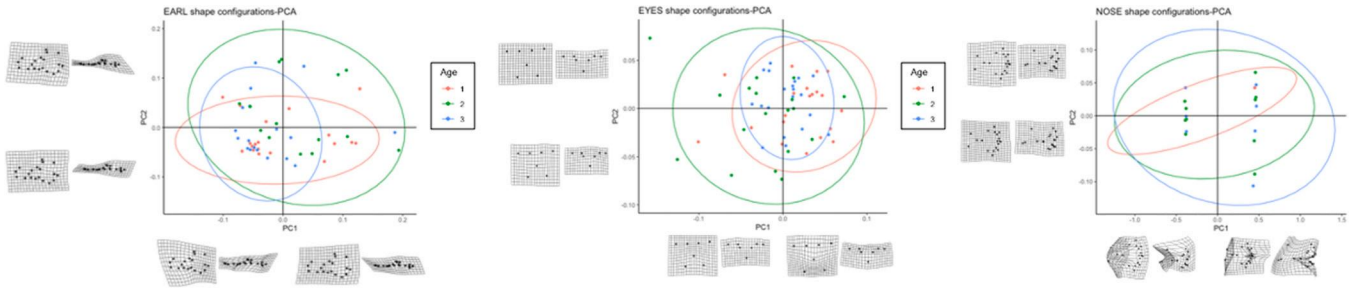

Fig. 15. PC 1 versus PC 2 of the French sample (EUR group) for age indicating the maximum and minimum of the shapes of the soft tissue left ear (left), eyes (middle), and nose (right) along PC 1. 1 = 18–29 years old; 2 = 30–44 years old; 3 = 45–59 years old.

59 years displayed a great amount of variation with slightly larger features observed. These findings are consistent with observations made by Guyomarc'h et al. [6], who found that age significantly influenced all matrices, except the superior hard-tissue facial matrix, of French individuals who were younger than 40 years old and those older than 40 years. Previous studies have also reported that South African individuals older than 60 years have larger centroid sizes for the left and right ears [44], which is consistent with our observations. The common consensus is that the external ear changes significantly with age, but the most substantial changes occur after 60 years [65,66]. Regarding age-related nasal shape changes, Schlager [36] reported that the nasal aperture widens with age in Chinese and European populations, which is consistent with our findings. Other studies have also reported age-related nasal prolongation and widening [71–73]. These changes may be due to downward gravitational forces that act on tissue that weaken with age [36].

Since our study aimed to determine whether different age groups should be pooled, we did not analyze the lower face or entire cranium individually, which are particularly affected by age-related changes [63]. In general, regional shapes overlapped considerably across age groups, suggesting that aging affects the soft tissue and the underlying skull substrate [63].

We observed that allometry heterogeneously affects soft tissue craniofacial morphology, causing variance in specific areas due to differences in growth and development patterns, which is consistent with the findings of Agbolade et al. [63]. We found that size influenced the morphology of the midface, both EAMs, and right orbit in white South Africans, whereas size influenced the eyes, nose, midface, right EAM, and both orbits in French individuals. In contrast, other studies focusing on white South Africans [44] reported that size significantly influenced only the left EAM. Our findings also contradict those of a French study in which allometry significantly influenced all matrices except the facial inferior matrix [6]. In a separate study, Schalger [36] found that the centroid sizes of nasal soft tissue were similar in Chinese and European populations but that the Chinese had slightly larger hard tissue configurations. For nasal features, population affinity seemed to have little influence on size. Allometry likely has a variable effect on soft tissue craniofacial morphology and may depend on growth and development patterns [63].

4.2. *Correlations between the underlying skull and soft-tissue face*

Based on the study results, hard tissue matrices were correlated with soft tissue matrices. This correlation was similar between the two populations, although the strengths of the association varied. Firstly, all soft tissue matrices (ears, eyes, nose, and mouth) were correlated to the midfacial matrix, the ears to the EAMs, and the nose to the anterior nasal aperture in both groups. These findings were expected given the interdependence of traits within an individual, which are affected similarly by functional and developmental factors [69]. Additionally, the pattern of correlation mostly followed anatomical logic [6], however the eyes were unexpectedly not correlated with the orbits, which might be due to a lack of standardized focus, and there only being two landmarks on the sides of the orbits. We also found stronger correlations between the hard and soft tissues of white South Africans than among the French. In a previous South African study [44], both ears were strongly correlated to their underlying EAMs, which is consistent with our findings. Ridel et al. [28,42] also reported significant correlations between nasal hard and soft tissue among South Africans, which is consistent with our findings. A French study [6] found significant correlations for the nose region and moderate correlations for the mouth, which contradicts our findings, which found moderate correlations for the nose and low/weak correlations for the mouth. However, comparable to Guyomarc'h et al. [6] we found moderate correlations for the ears and relatively low correlations

Table 6
Hard and soft tissue shape changes associated with size in the complete sample and within each population.

		Complete sample							White South African						French			
		Size		Pop* Size		Sex* Size		Pop*Sex* Size	Size		Sex* Size		Size		Sex* Size	
		$Test^3$	$Test^4$	$Test^3$	$Test^4$	$Test^3$	$Test^4$	$Test^3$	$Test^4$	$Test^3$	$Test^4$	$Test^3$	$Test^4$	$Test^3$	$Test^4$	$Test^3$	$Test^4$
Soft-tissue	Left ear	0.146	0.146	0.695	0.695	0.384	0.384	0.577	0.577	0.765	0.765	0.910	0.909	0.835	0.835	0.513	0.513
	Right ear	0.323	0.323	0.905	0.905	0.785	0.785	0.896	0.897	0.071	0.070.	0.757	0.757	0.197	0.197	0.598	0.598
	Eyes	**1.390e−05** ***	**1.386e−05** ***	0.703	0.703	0.098	0.097	0.640	0.640	0.596	0.596	0.111	0.111	**0.003****	**0.003****	0.210	0.210
	Nose	**3.050e−05** ***	**3.047e−05** ***	**0.001****	**0.001****	**0.016***	**0.016***	0.574	0.574	0.287	0.287	**0.049***	**0.049***	**6.330e−13** ***	**6.330e−13** ***	0.112	0.112
	Mouth	**0.043***	**0.043***	0.140	0.140	0.462	0.462	**0.013***	**0.013***	0.088	0.088.	0.181	0.181	0.132	0.132	0.059	0.059
Hard-tissue	Midfacial matrix	**8.740e−06** ***	**8.740e−06** ***	0.091	0.091	0.574	0.574	0.712	0.712	**0.021***	**0.021***	0.232	0.232	**0.003****	**0.003****	0.973	0.973
	Left EAM	0.152	0.152	**3.360e−05** ***	**3.361e−05** ***	**4.010e−4** ***	**4.006e−4** ***	**0.031***	**0.031***	**0.005****	**0.005****	**0.004****	**0.004****	0.387	0.388	0.677	0.677
	Right EAM	**0.021***	**0.021***	**0.019***	**0.019***	0.379	0.379	0.706	0.706	**0.032 ***	**0.031***	0.804	0.804	**0.044***	**0.044***	0.579	0.579
	Left orbit	**4.800e−4 ***	**4.800e−4 ***	0.322	0.322	0.404	0.404	0.494	0.494	0.206	0.206	0.357	0.357	**0.004****	**0.004****	0.432	0.432
	Right orbit	**0.017***	**0.017***	0.121	0.121	0.389	0.389	0.227	0.227	**0.027***	**0.027***	0.877	0.877	**3.700e−05** ***	**3.701e−05** ***	0.200	0.200
	Nasal aperture	0.086	0.086	0.389	0.389	0.705	0.705	0.881	0.881	0.122	0.123	0.558	0.558	0.825	0.825	0.5431	0.543

$Test^3$ = 50–50 MANOVA $Test^4$= MANCOVA. Significant p-values ($p < 0.05$) are indicated in bold. **= p-values less that 0.01 and *** = p-values less than 0.001. EAM, external auditory meatus

for the eyes. This variation may be attributed to landmark non-coplanarity, which can result in inconsistent specimens relative to the digitization plane or difficulties identifying landmark loci [63]. Furthermore, the patterns of morphological integration are not always simple, and classifications typically only account for a fraction of adult variation [69,74,71,72].

As shown in our French group, soft tissues may not follow underlying structures as precisely as expected.

Overall, facial shape variation is evidently influenced by population differences, sexual dimorphism, and aging. Despite each group being unique, especially with regard to the mouth, nose, and internal and external auditory regions, the study results are significant in CFR because they establish a baseline for facial morphologic standards for each population. This research can be used to create normative databases that forensic scientists, anthropologists, orthodontists, reconstructive surgeons, and others can use to predict soft tissue facial profiles from underlying skulls or treatments for specific populations. Given the scarcity of research on hard and soft tissue facial variation in South African and French populations, as well as the different approaches used to characterize this variation, such as surface model analysis using 3D landmarks, our results cannot be generalized to other populations. Further, comparing our results with other studies was challenging due to different assessment criteria being used and few studies using similar facial matrices as investigated in our study.

5. Conclusion

The evolution and progression of CFR techniques and their practical applications have unveiled extensive diversity among and across populations and are instrumental in creating reliable standards tailored to specific populations. Our study delved into the intricacies of facial variation among white South African and French individuals, using a comprehensive database and 3D imaging technology to analyze the effects of sexual dimorphism, aging, and population affinity. Through detailed analysis of 3D landmarks encompassing both facial hard and soft tissue, this study revealed the distinct interaction between these factors, offering invaluable insights for forensic practitioners and anthropologists alike.

The primary focus of this investigation was elucidating the effect of population affinity on facial features, thereby facilitating the creation of reconstructions tailored to specific population groups. This understanding is pivotal in forensic endeavors where accurately identifying individuals from diverse backgrounds is imperative. By discerning the distinct morphological traits associated with different populations, practitioners can craft reconstructions that capture the unique characteristics inherent to each group, thereby augmenting the precision of identifications.

Moreover, our analysis of sexual dimorphism illuminated the inherent disparities in facial morphology between males and females within specific population groups. Equipped with this information, forensic practitioners can refine reconstructions to accommodate the population-specific characteristic features exhibited by males and females, thus refining the accuracy of identifications. Additionally, the exploration of the impact of aging on facial morphology in this study yielded invaluable insights into the dynamic nature of facial features over time. By comprehending the trajectory of facial changes associated with aging, practitioners can adjust their reconstructions to reflect age-related alterations, strengthening the accuracy of identifications across various age demographics.

Furthermore, our investigation examined the complex correlation between underlying skull structures and soft tissue features, offering a deeper comprehension of their interrelationship. By establishing robust correlations between hard tissue matrices and soft tissue matrices, practitioners can predict soft tissue features based on underlying skeletal morphology, thereby enhancing the fidelity of reconstructions to the deceased individual's facial characteristics. Overall, this study

Table 7
Results of correlation between hard and soft tissue and its dependency on population affinity.

	White South African								French							
	Midfacial matrix		Left EAM		Right EAM		Nasal aperture		Midfacial matrix		Left EAM		Right EAM		Nasal aperture	
	P-value	r^2-PLS	P-value	r^2-PLS	P-value	r^2-PLS	P-value	r^2-PLS	P-value	r^2-PLS	P-value	r^2-PLS	P-value	r^2-PLS	P-value	r^2-PLS
Left ear	**0.001**	0.863	**0.001**	0.871	-	-	-	-	0.580	0.419	0.628	0.391	0.648	0.400	-	-
Right ear	**0.001**	0.874	-	-	**0.001**	0.875	-	-	0.719	0.384	0.247	0.416	**0.027**	0.499	-	-
Eyes	**0.001**	0.669	-	-	-	-	-	-	0.780	0.290	-	-	-	-	-	-
Nose	**0.001**	0.933	-	-	-	-	**0.001**	0.976	0.386	0.456	-	-	-	-	0.051	0.510
Mouth	0.132	0.464	-	-	-	-	-	-	0.231	0.367	-	-	-	-	-	-

Significant correlation between hard tissue and soft tissue tested by two-blocks Partial Least Square analyses. Bold p-values ($p<0.05$) indicate statistical significance. EAM, external auditory meatus

emphasizes the importance for a nuanced understanding of craniofacial variations across diverse populations and highlights the critical role of demographic factors such as population affinity, sex, and age in the creation and application of CFR methods.

By defining the complex interrelationships between these factors and craniofacial morphology, our study emphasizes the necessity for tailored approaches that account for population-specific variations. Moreover, it elucidates that overlooking these demographic considerations can compromise the accuracy and reliability of craniofacial reconstructions. Thus, our findings underscore the importance of adopting comprehensive methodologies that integrate demographic factors to ensure the precision and validity of craniofacial analyses and reconstructions within forensic, anthropological, and clinical contexts.

Lastly, while population affinity, sexual dimorphism, and aging have been demonstrated to characterize craniofacial shape, facial morphology is also influenced by hormonal influences, inherent genetic factors, and environmental variation or functional demands [69,75]. This comprehensive understanding expands the horizons of forensic practice, allowing for nuanced reconstructions that encapsulate the myriad influences contributing to facial variability. Moreover, by employing GMM, this research revealed subtle yet significant patterns of facial variability, which might not be readily discernible through traditional morphometric methods. This approach not only simplifies the process of data collection and evaluation but also facilitates the visualization of shape changes, thereby offering a more comprehensive understanding of facial diversity across populations. By amalgamating these tools, our research establishes a holistic framework for quantifying and comprehending facial variation between populations.

Author contributions

Category 1

Conception and design of study: TM Mbonani, AF Ridel, EN L'Abbé

Acquisition of data: TM Mbonani, AF Ridel, EN L'Abbé

Analysis and/or interpretation of data: TM Mbonani, AF Ridel, EN L'Abbé

Category 2

Drafting the manuscript: TM Mbonani, AF Ridel, EN L'Abbé

Revising the manuscript critically for important intellectual content: TM Mbonani, AF Ridel, EN L'Abbé

Category 3

Approval of the version of the manuscript to be published (the names of all authors must be listed): TM Mbonani, AF Ridel, EN L'Abbé

Funding

The University of Pretoria, South Africa, provided funding for this research through the UP Postgraduate Masters Research Bursary.

CRediT authorship contribution statement

Thandolwethu Mbali Mbonani: Writing – review & editing, Writing – original draft, Visualization, Methodology, Investigation, Funding acquisition, Formal analysis, Data curation, Conceptualization. **Alison Fany Ridel:** Writing – review & editing, Writing – original draft, Visualization, Supervision, Methodology, Investigation, Formal analysis, Data curation, Conceptualization. **Ericka Noelle L'Abbé:** Writing – review & editing, Writing – original draft, Supervision, Formal analysis, Data curation, Conceptualization.

Declaration of Competing Interest

None.

Acknowledgments

The authors would like to thank Prof. Uys and Dr. Botha from the Oral and Dental Hospital, University of Pretoria, South Africa, and Groenkloof Hospital, South Africa, for providing access to their CBCT databases. The University of Bordeaux in France is thanked for providing French CBCT data as part of the *Bakeng se Afrika* initiative. We thank Meg-Kyla Erasmus (prior researcher: MSc dissertation) for allowing us to use shape data gathered in a previous research study at the University of Pretoria. Thank you to Dr Cheryl Tosh for editing.

Appendix A. Supporting information

Supplementary data associated with this article can be found in the online version at doi:10.1016/j.forsciint.2024.112282.

References

[1] Mashigo L. There are an estimated 7 000 unidentified bodies in South Africa's medico-legal laboratories; 2023. Available from: ⟨https://www.iol.co.za/the-star/news/there-are-are-an-estimated-7-000-unidentified-bodies-in-south-africas-medico-legal-laboratories-7f419c2c-69e8-4fe5-863e-bc855f9cc008⟩.

[2] P. Claes, D. Vandermeulen, S. De Greef, G. Willems, J.G. Clement, P. Suetens, Computerized craniofacial reconstruction: conceptual framework and review, Forensic Sci. Int 201 (1-3) (2010) 138–145, https://doi.org/10.1016/j.forsciint.2010.03.008.

[3] S. De Greef, D. Vandermeulen, P. Claes, P. Suetens, G. Willems, The influence of sex, age and body mass index on facial soft tissue depths, Forensic Sci. Med Pathol. 5 (2) (2009) 60–65, https://doi.org/10.1007/s12024-009-9085-9.

[4] E. Simpson, M. Henneberg, Variation in soft-tissue thicknesses on the human face and their relation to craniometric dimensions, Am. J. Phys. Anthr. 118 (2) (2002) 121–133, https://doi.org/10.1002/ajpa.10073.

[5] J.B. Schimmler, R.P. Helmer, J. Rieger, Craniometric individuality of human skulls. Forensic analysis of the skull: craniofacial analysis, reconstruction and identification, John Wiley & Sons, Nashville, TN, 1993.

[6] P. Guyomarc'h, B. Dutailly, J. Charton, F. Santos, P. Desbarats, H. Coqueugniot, Anthropological facial approximation in three dimensions (AFA3D): computer-assisted estimation of the facial morphology using geometric morphometrics, J. Forensic Sci. 59 (6) (2014) 1502–1516, https://doi.org/10.1111/1556-4029.12547.

[7] C.N. Stephan, Anthropological facial 'reconstruction' – recognizing the fallacies, 'unembracing' the errors, and realizing method limits, Sci. Justice 43 (4) (2003) 193–200, https://doi.org/10.1016/S1355-0306(03)71776-6.

[8] A.J. Tyrrell, M.P. Evison, A.T. Chamberlain, M.A. Green, Forensic three-dimensional facial reconstruction: historical review and contemporary developments, J. Forensic Sci. 42 (4) (1997) 14176J, https://doi.org/10.1520/JFS14176J.

[9] L. Verzé, History of facial reconstruction, Acta Biol. Med 80 (2009) 5–12.

[10] H. Ullrich, C.N. Stephan, On Gerasimov's Plastic Facial Reconstruction Technique: new Insights to Facilitate Repeatability, J. Forensic Sci. 56 (2) (2011) 470–474, https://doi.org/10.1111/j.1556-4029.2010.01672.x.

[11] C. Wilkinson, Facial reconstruction – anatomical art or artistic anatomy? J. Anat. 216 (2) (2010) 235–250, https://doi.org/10.1111/j.1469-7580.2009.01182.x.

[12] D. Vandermeulen, P. Claes, S.D. Greef, G. Willems, J. Clement, S. Paul, Automated facial reconstruction. Craniofacial identification, Cambridge University Press, Cambridge, 2012, pp. 203–221.

[13] S. Gupta, Forensic facial reconstruction: the final frontier, JCDR (2015), https://doi.org/10.7860/JCDR/2015/14621.6568.

[14] S.D. Greef, G. Willems, Three-dimensional Cranio-Facial Reconstruction in Forensic Identification: latest Progress and New Tendencies in the 21st Century, J. Forensic Sci. 50 (1) (2005) 1–5, https://doi.org/10.1520/JFS2004117.

[15] S. De Greef, P. Claes, W. Mollemans, D. Vandermeulen, P. Suetens, G. Willems, Computer-assisted facial reconstruction: recent developments and trends, Rev. Belg. Med Dent. 60 (2005) 237–249.

[16] C. Wilkinson, Computerized forensic facial reconstruction: a review of current systems, FSMP 1 (3) (2005) 173–178, https://doi.org/10.1385/FSMP:1:3:173.

[17] P. Claes, D. Vandermeulen, S. De Greef, G. Willems, P. Suetens, Craniofacial reconstruction using a combined statistical model of face shape and soft tissue depths: methodology and validation, Forensic Sci. Int 159 (2006) S147–S158, https://doi.org/10.1016/j.forsciint.2006.02.035.

[18] J.M. Starbuck, R.E. Ward, The affect of tissue depth variation on craniofacial reconstructions, Forensic Sci. Int 172 (2-3) (2007) 130–136, https://doi.org/10.1016/j.forsciint.2007.01.006.

[19] K. Kreutz, M.A. Verhoff, Forensic Facial Reconstruction – Identification based on Skeletal Findings, Dtsch Ärztebl 107 (2007) 1160–1165.

[20] S. Schlager, A. Rüdell, Analysis of the human osseous nasal shape-population differences and sexual dimorphism: human osseous Nasal Shape, Am. J. Phys. Anthr. 157 (2015) 571–581, https://doi.org/10.1002/ajpa.22749.

[21] M.L. Moss, R.W. Young, A functional approach to craniology, Am. J. Phys. Anthr. 18 (4) (1960) 281–292, https://doi.org/10.1002/ajpa.1330180406.

[22] W.R. Atchley, B.K. Hall, A model for development and evolution of complex morphological structures, Biol. Rev. 66 (2) (1991) 101–157, https://doi.org/10.1111/j.1469-185X.1991.tb01138.x.

[23] D.H. Enlow, M.G. Hans, Essentials of facial growth, Saunders, Philadelphia, 1996.

[24] D.E. Lieberman, B.M. McBratney, G. Krovitz, The evolution and development of cranial form in Homo sapiens, Proc. Natl. Acad. Sci. USA 99 (3) (2002) 1134–1139, https://doi.org/10.1073/pnas.022440799.

[25] C.P. Klingenberg, M. Barluenga, A. Meyer, Shape analysis of symmetric structures: quantifying variation among individuals and asymmetry, Evolution 56 (10) (2002) 1909–1920, https://doi.org/10.1111/j.0014-3820.2002.tb00117.x.

[26] Y. Tomoyasu, T. Yamaguchi, A. Tajima, T. Nakajima, I. Inoue, K. Maki, Further evidence for an association between mandibular height and the growth hormone receptor gene in a Japanese population, Am. J. Orthod. Dentofac. Orthop. 136 (4) (2009) 536–541, https://doi.org/10.1016/j.ajodo.2007.10.054.

[27] F. Gröning, M. Fagan, P. O'higgins, Comparing the distribution of strains with the distribution of bone tissue in a human mandible: A finite element study, Anat. Rec. 296 (1) (2013) 9–18, https://doi.org/10.1002/ar.22597.

[28] A. Ridel, An automated computer-assisted approximation of the nose in South Africans from CBCT (cone beam computed tomography) scans, University of Pretoria, 2018.

[29] A.F. Ridel, F. Demeter, M. Galland, E.N. L'Abbé, D. Vandermeulen, A.C. Oettlé, Automatic landmarking as a convenient prerequisite for geometric morphometrics. Validation on cone beam computed tomography (CBCT)- based shape analysis of the nasal complex, Forensic Sci. Int 306 (2020) 110095, https://doi.org/10.1016/j.forsciint.2019.110095.

[30] G.C. Krüger, E.N. L'Abbé, K.E. Stull, M.W. Kenyhercz, Sexual dimorphism in cranial morphology among modern South Africans, Int J. Leg. Med 129 (4) (2015) 869–875, https://doi.org/10.1007/s00414-014-1111-0.

[31] P.Z. Zedníková Malá, V. Krajíček, J. Velemínská, How tight is the relationship between the skeletal and soft-tissue facial profile: A geometric morphometric analysis of the facial outline, Forensic Sci. Int 292 (2018) 212–223, https://doi.org/10.1016/j.forsciint.2018.09.014.

[32] C.F. Spoor, F.W. Zonneveld, G.A. Macho, Linear measurements of cortical bone and dental enamel by computed tomography: applications and problems, Am. J. Phys. Anthr. 91 (4) (1993) 469–484, https://doi.org/10.1002/ajpa.1330910405.

[33] P.J. Scheinder, D. Elberly, Geometric tools for computer graphics, Elsevier Science Inc, New York, 2002.

[34] P. Mitteroecker, P. Gunz, Advances in geometric morphometrics, Evol. Biol. 36 (2) (2009) 235–247, https://doi.org/10.1007/s11692-009-9055-x.

[35] G. Ocakoğlu, S. Turan Özdemİr, İ. Ercan, Etöz A. The shape of the external human ear: a geometric morphometric study. Turk. Klin. J. Med Sci. 33 (1) (2013) 184–190, https://doi.org/10.5336/medsci.2012-30150.

[36] S. Schlager, Soft-tissue reconstruction of the human nose: population differences and sexual dimorphism = Weichteilrekonstruktion der menschlichen Nase: Populationsunterschiede und Sexualdimorphismus, Universität Freiburg, 2013.

[37] J. Caple, C.N. Stephan, A standardized nomenclature for craniofacial and facial anthropometry, Int J. Leg. Med 130 (3) (2016) 863–879, https://doi.org/10.1007/s00414-015-1292-1.

[38] P. Gunz, P. Mitteroecker, Semilandmarks: a method for quantifying curves and surfaces, Hystrix Ital. J. Mammal. 24 (2013), https://doi.org/10.4404/hystrix-24.1-6292.

[39] T.D. White, P.A. Folkens, The human bone manual, Elsevier Academic, Amsterdam, Boston, 2005.

[40] V.F. Ferrario, C. Sforza, A. Anderbegani, C.E. Poggio, L.L. Dalloca, Relative position of porion and tragus in orthodontic patients, Clin. Anat. 8 (5) (1995) 352–358, https://doi.org/10.1002/ca.980080508.

[41] F. Lundström, A. Lundström, Natural head position as a basis for cephalometric analysis, Am. J. Orthod. Dentofac. Orthop. 101 (3) (1992) 244–247, https://doi.org/10.1016/0889-5406(92)70093-P.

[42] A.F. Ridel, F. Demeter, E.N. L'abbé, D. Vandermeulen, A.C. Oettlé, Nose approximation among South African groups from cone-beam computed tomography (CBCT) using a new computer-assisted method based on automatic landmarking, Forensic Sci. Int 313 (2020) 110357, https://doi.org/10.1016/j.forsciint.2020.110357.

[43] T. Mbonani, A. Hagg, E. L'Abbé, A. Oettlé, A. Ridel, Validation of the utilisation of automatic placement of anatomical and sliding landmarks on three-dimensional models for shape analysis of human pelves, Forensic Imaging 33 (2023) 200542, https://doi.org/10.1016/j.fri.2023.200542.

[44] M.-K. Erasmus, E.N. L'Abbé, A.F. Ridel, A geometric morphometric assessment of the hard tissue external auditory meatus and soft tissue ear of South Africans, Forensic Sci. Int Rep. 8 (2023) 100331, https://doi.org/10.1016/j.fsir.2023.100331.

[45] P.D. de Wet, A geometric morphometric (GMM) study on variations in the French population's soft- and hard-tissue morphology matrices for forensic implications using Computed Tomography (CT) scans (Hons research), University of Pretoria, 2022.

[46] D.E. Slice, Geometric morphometrics, Annu Rev. Anthr. 36 (1) (2007) 261–281, https://doi.org/10.1146/annurev.anthro.34.081804.120613.

[47] D.G. Kendall, Shape manifolds, procrustean metrics, and complex projective spaces, Bull. Lond. Math. Soc. 16 (2) (1984) 81–121, https://doi.org/10.1112/blms/16.2.81.

[48] I.L. Dryden, K.V. Mardia, Statistical shape analysis with applications in R. 2nd ed, John Wiley & Sons, Chichester, UK; Hoboken, NJ, 2016.

[49] J.C. Gower, Generalized Procrustes analysis, Psychometrika 40 (1) (1975) 33–51, https://doi.org/10.1007/BF02291478.

[50] F.J. Rohlf, D. Slice, Extensions of the Procrustes method for the optimal superimposition of landmarks, Syst. Zool. 39 (1) (1990) 40, https://doi.org/10.2307/2992207.

[51] P. Mitteroecker, P. Gunz, S. Windhager, K. Schaefer, A brief review of shape, form, and allometry in Geometric morphometrics, with applications to human facial morphology, Hystrix it J. Mamm. 24 (2013) 59–66, https://doi.org/10.4404/hystrix-24.1-6369.

[52] J. Claude, M. Stayton, M. Baylac, Traditional statistics for geometric morphometrics. In: Use R!. Morphometrics with R., Springer, New York, 2008.

[53] L. Scrucca, Assessing multivariate normality through interactive dynamic graphics, Quad. Stat. 2 (2000) 221–240.

[54] Schlager S. Calculations and visualisations related to geometric morphometrics; 2017..

[55] A. Rosas, M. Bastir, Thin-plate spline analysis of allometry and sexual dimorphism in the human craniofacial complex, Am. J. Phys. Anthr. 117 (3) (2002) 236–245, https://doi.org/10.1002/ajpa.10023.

[56] E.H. Kimmerle, A. Ross, D. Slice, Sexual dimorphism in America: geometric morphometric analysis of the craniofacial region, J. Forensic Sci. 53 (1) (2008) 54–57, https://doi.org/10.1111/j.1556-4029.2007.00627.x.

[57] F.J. Rohlf, M. Corti, Use of two-block partial least-squares to study covariation in shape, Syst. Biol. 49 (4) (2000) 740–753, https://doi.org/10.1080/106351500750049806.

[58] R Core Team. R: a language and environment for statistical computing. Vienna, Austria: R Foundation for Statistical Computing; 2015.

[59] Schlager S., Jefferis G., Dryden I. Calculations and visualisations related to geometric morphometrics; 2020.

[60] Adams D.C., Collyer M., Kaliontzopoulou A., Baken E. Geometric Morphometric analyses of 2D/3D landmark data; 2022..

[61] O. Langsrud, 50-50 multivariate analysis of variance for collinear responses, J. R. Stat. Soc. D. 51 (3) (2002) 305–317, https://doi.org/10.1111/1467-9884.00320.

[62] Langsrud Ø., Mevik B.H. Fifty-fifty MANOVA (ffmanova); 2012..

[63] O. Agbolade, A. Nazri, R. Yaakob, A.A. Ghani, Y.K. Cheah, Morphometric approach to 3D soft-tissue craniofacial analysis and classification of ethnicity, sex, and age, PLOS ONE 15 (4) (2020) e0228402, https://doi.org/10.1371/journal.pone.0228402.

[64] S. Ritz-Timme, P. Gabriel, J. Tutkuviene, P. Poppa, Z. Obertová, D. Gibelli, et al., Metric and morphological assessment of facial features: A study on three European populations, Forensic Sci. Int 207 (1-3) (2011), https://doi.org/10.1016/j.forsciint.2011.01.035.

[65] C. Sforza, G. Grandi, M. Binelli, D.G. Tommasi, R. Rosati, V.F. Ferrario, Age- and sex-related changes in the normal human ear, Forensic Sci. Int 187 (1-3) (2009), https://doi.org/10.1016/j.forsciint.2009.02.019.

[66] K.S. Alexander, D.J. Stott, B. Sivakumar, N. Kang, A morphometric study of the human ear, J. Plast. Reconstr. Aesthet. Surg. 64 (1) (2011) 41–47, https://doi.org/10.1016/j.bjps.2010.04.005.

[67] R. Azaria, N. Adler, R. Silfen, D. Regev, D.J. Hauben, Morphometry of the adult human earlobe: a study of 547 subjects and clinical application, Plast. Reconstr. Surg. 111 (7) (2003) 2398–2402, https://doi.org/10.1097/01.PRS.0000060995.99380.DE.
[68] J.L. McDowell, M.W. Kenyhercz, E.N. L'Abbé, An evaluation of nasal bone and aperture shape among three South African populations, Forensic Sci. Int 252 (2015), https://doi.org/10.1016/j.forsciint.2015.04.016.
[69] A. Farrera, M. García-Velasco, M. Villanueva, Quantitative assessment of the facial features of a Mexican population dataset, Forensic Sci. Int 262 (2016), https://doi.org/10.1016/j.forsciint.2016.02.046.
[70] M. Steyn, E.N. L'Abbé, J. Myburgh, Forensic anthropology as practiced in South Africa. Handbook of forensic anthropology and archaeology, 2nd ed., Routledge, London, 2016.
[71] F. Chen, Y. Chen, Y. Yu, Y. Qiang, M. Liu, D. Fulton, et al., Age and sex related measurement of craniofacial soft tissue thickness and nasal profile in the Chinese population, Forensic Sci. Int 212 (1-3) (2011), https://doi.org/10.1016/j.forsciint.2011.05.027.
[72] C. Sforza, G. Grandi, M. De Menezes, G.M. Tartaglia, V.F. Ferrario, Age- and sex-related changes in the normal human external nose, Forensic Sci. Int 204 (1-3) (2011), https://doi.org/10.1016/j.forsciint.2010.07.027.
[73] E. Nikita, Age-associated variation and sexual dimorphism in adult cranial morphology: implications in anthropological studies, Int J. Osteoarchaeol 24 (5) (2014) 557–569, https://doi.org/10.1002/oa.2241.
[74] A. Damon, C.C. Seltzer, H.W. Stoudt, B. Bell, Age and physique in healthy White veterans at Boston, J. Gerontol. 27 (2) (1972) 202–208, https://doi.org/10.1093/geronj/27.2.202.
[75] J.M. Cheverud, Developmental integration and the evolution of pleiotropy, Am. Zool. 36 (1) (1996) 44–50, https://doi.org/10.1093/icb/36.1.44.